CALIFORNIA STATE UNIVERSITY, NORTHRIDGE

SURFACE AND AIR TEMPERATURE RELATIONSHIPS:

A MICROCLIMATE, URBAN HEAT ISLAND STUDY

OF THE

CSUN CAMPUS

A thesis submitted in partial fulfillment of the requirements

For the degree of Master of Arts in

Geography

By

Mark Jacobi

May 2014

The thesis of Mark Jacobi is approved:

Shawna Dark, Ph.D.	Date
Steve Graves, Ph.D.	Date
Helen Cox, Ph.D., Chair	Date

California State University, Northridge

Acknowledgments

I would like to thank my committee members who supported my efforts in writing this thesis.

To my chair, Dr. Helen Cox,

To Dr. Shawna Dark,

To Dr. Steve Graves,

These professors have been instrumental in assisting me throughout my academic journey at CSUN. I would also like to extend my gratitude to the entire CSUN Geography Department, especially to Amalie Orme, Julie Laity, Yiffei Sun, Darrick Danta, Ed Jackiewicz, James Craine, Soheil Boroushaki, Eli Bartle, my fellow grad students and the Tamburro family.

In addition to my academic assistants and comrades, I would like to add special recognition to my family and friends that have supported me at all stages of my studies, specifically Michael Battin, and Eric Wilson for their incredible support during my studies at CSUN.

Table of Contents

List of Figures

List of Tables

Abstract

Surface and Air Temperature Relationships:

A Microclimate, Urban Heat Island Study of the CSUN Campus

By

Mark Jacobi

Master of Arts in

Geography

Heat waves, on average, are responsible for more deaths annually than all other kinds of weather combined. In some instances, excessive heat is exacerbated by what is commonly known as the “urban heat island” effect, which arises from changes in the thermal properties of land surfaces which accompany urbanization. The instances of deadly heatwaves are expected to increase as a consequence of the climate changes that accompany the rising levels of carbon dioxide and other heat trapping gases in the atmosphere. In this study, the effect of surface type on temperature is assessed through a case study carried out at California State University, Northridge through the deployment of air temperature data loggers. The surfaces surrounding each sensor were classified by the percentage of impervious surface cover within ten meters of each sensor. Correlation analyses were performed to assess the relationships between warmer temperatures and increased percentages of impervious surface cover. The sensors were also grouped into four classes depending on the percentage of the impervious surface cover in their

vicinities. A moderately strong correlation was observed between air temperatures and impervious surface cover. The grouped analysis displayed the same pattern but the most significant effect was the occurrence of significantly cooler temperatures over the least impervious surfaces. Areas with the most impervious surfaces were warmer much of the time, while areas of intermediate permeability showed no statistically significant trend.

1 Introduction

The widespread use of fossil fuels over the last century has caused an increase in the concentration of carbon dioxide in the atmosphere. Because carbon dioxide traps heat, this increase has raised the average global air temperature by 0.76° Celsius since 1850 when temperature records began (IPCC 2007). Most scientists expect the trend to continue, and possibly accelerate, as our energy habits continue to release additional "greenhouse" gases into the atmosphere. This is one way in which human activities are affecting weather as well as the global climate system.

In addition to these atmospheric changes, surface alterations also impact temperatures and weather because of their effects on albedo, evapotranspiration, thermal capacities and other components of the energy exchanges in more localized environments. Urbanization is a process which results in increased areas of land covered by roads, buildings, and other features that have these impacts and is one example of this kind of human impact. These changes often result in higher temperatures in places where cities have been constructed. In addition, human activities in these areas also produce waste heat which contributes to the phenomenon (Arnfield 2003).

These changes often lead to what is commonly known as the "urban heat island" (UHI) effect. Urban areas have grown considerably in both size and number during the last century. In fact, more than half the world's population now lives in urban areas compared to only twenty percent in the early 1900s. The United Nations Department of Social and Economic Affairs predicts that this growth pattern will continue (United Nations 2010). This shift in population from rural to urban areas means that more people

are likely to experience some of the negative consequences of UHIs than before. This is important because UHIs can amplify the effects of extremely hot weather, and extreme heat events already cause more fatalities than all other weather events combined (United States Centers for Disease Control and Prevention 2010). Besides causing increased mortality, excessive heat increases air pollution and raises energy demands (Katsouyanni, Pantazopoulou and Touloumi 1993) so there are many reasons to study the effects that our built environment has on our immediate living areas.

The purpose of this study is to examine the relationships between impervious surfaces and air temperatures. Specifically it aims to identify whether UHI effects are being generated due to areas of reduced permeability such as asphalt, concrete and other impervious surface features. Additionally, this study seeks to determine how large naturally landscaped areas, which are mostly pervious, may reduce temperatures or mitigate UHI effects, especially during periods of extremely warm weather. This study was conducted on the California State University, Northridge (CSUN) campus in Los Angeles, California between July 2, and July 15, 2012.

The main focus of this paper is to answer these research questions:

- What is the relationship between the area of impervious surfaces and the air temperatures on the CSUN campus?
- Is there evidence of UHI development during periods of warm weather?

2 Literature Review

2.1 Urban Heat Islands

The UHI effect was first described by Luke Howard in London (1833). His observation was simple: air temperatures in London were often warmer than the surrounding countryside. Even though the concept has been documented since that time, urban climate studies are a fairly recent development.

While the UHI as a concept is fairly straight forward, there are several ways to describe it and it operates on many spatial scales. In 1976, Dr. T.R. Oke broke the UHI phenomena into three different parts in order to address them more clearly. The surface heat island (SHI) exists at the surface due to solar heating during the day. Just above the SHI is the urban canopy layer (UCL). The UCL is generally found from the ground to the height of the buildings and trees. This layer involves the direct heat exchange between objects on the surface and the atmosphere making it very important to study because it is the layer in which people generally experience weather conditions. Above that layer is the urban boundary layer which describes the air above the UCL to a height which varies according to time of day and season, and is generally a more regional feature of the UHI. Examples of those features are displayed in figure 1. That image displays the larger scale UHI on top and then illustrates how the other types of UHI's relate to that larger scale feature. The focus of this study is on the UCL type of heat island.

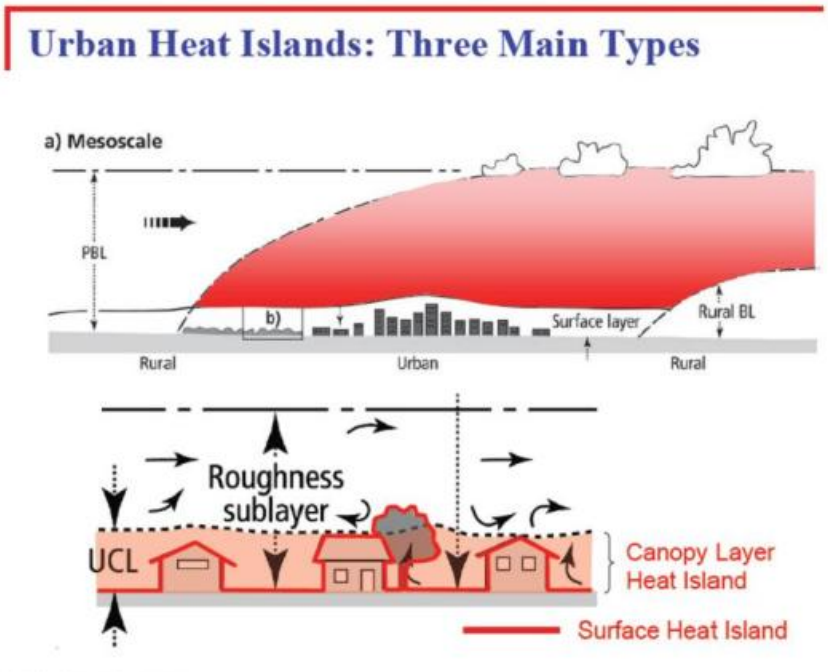

Figure 1. Urban Heat Island Types as discussed by Oke (1976) as presented in the Fabrizi et al. study (2010). While heat islands may exist on the ground or above an area, the focus of this study is on the urban canopy layer (UCL) which exists above the ground to the height of buildings and trees.

2.2 Early Studies and Methods

Since their discovery, several ways of studying the UHI phenomena have been implemented. Because of their spatial nature, one of the longest standing and most traditional methods of investigating UHIs has been simply comparing the temperatures from in situ weather stations within and outside urban areas (Runnalls and Oke 2000). This approach suffers from issues associated with spatial resolution, most weather stations are quite distant from each other, so gross interpolations are made between data points, which do not reflect many of the features contributing to those urban heat islands (Runnalls and Oke 2000). Pioneering studies by Fassig (1907), Saucier (1949), and

Bigler/Ligda (1956) examined possible downwind effects of large urban areas which were later followed by studies by Woolum and Canfield in 1968 describing more localized urban effects near Washington DC. By then it was widely accepted that human activities were affecting the weather in some locations and those beliefs were confirmed when Changnon (1968) documented increases in precipitation downwind of the urbanized region of Chicago.

One early ambitious UHI study, the METROMEX field project, was done in St. Louis, Missouri in 1971 (Sullivan 2009). This study used more than 200 rain gages distributed evenly over an area of about 5,700 square kilometers. It began with seven temperature stations and the number of stations increased to twenty five by the end of the five year study. Even though a relationship between urban areas and increased precipitation and temperatures was documented in the METROMEX study, Sullivan points out that the small number of temperature recording stations greatly limited that team's ability to correlate many heat island effects with changes in weather. He concludes that a larger number of strategically placed stations are needed to adequately assess the effects of UHI. Such methodology is indicative of previous UHI studies. Although it is convenient to make use of previously existing weather stations, their locations are not conducive to the study of the effects of UHI. The convenience of using existing stations combined with the financial savings is counterbalanced by studies of limited value.

UHI studies have also involved recording air temperatures along transect lines through both rural and urban areas. One such study was done in Australia which showed a positive correlation between population size and UHI development (Torok, et al. 2001).

Another study was conducted in Phoenix which used both transect lines and in situ weather stations to demonstrate UHI patterns in that city (Hedquist 2006). While these studies had better spatial resolution, they lost temporal resolution since the temperatures were not all recorded simultaneously. Another similar study was done in Athens and used temperature recorders mounted on automobiles which drove along routes around and through a large green park area (Zoulia, Santamouris and Dimoudi 2009). The goal of their approach was to locate cooler temperatures within the documented heat island. While they did detect some cooling, their results were inconclusive, partly because they drove on roads to get the data instead of on the grassy parts of the park. In Australia, another study using driven transect sampling was conducted (Torok, et al. 2001). That study demonstrated a positive correlation between the town's population size and UHI effects, and confirmed that small towns also created UHIs. While the use of mobile transects for UHI studies has proven quite useful, there is a drawback in that the data are often not recorded simultaneously, hence their temporal resolution suffers. This can be resolved, however, by setting data loggers out along transects that do gather the information simultaneously. For instance, in a Singapore study, which was commissioned to study the effects of a high rise development, sensors were deployed along transect lines (Balazs, et al. 2009). Many different types of meteorological data were sampled in that study which contrasted weather differences between a high density row of developments and a nearby open area. Those data were also used in conjunction with numerical models and computer software systems which have become much more common with the advent of new technologies.

2.3 Space Age Technologies

Advances in remote sensing technology since the 1970s have greatly increased our ability to study the UHI phenomenon. A 1976 study using remotely sensed imagery was done showing UHI patterns in Baltimore, Maryland, with correlation analyses on land cover and type use (Pease, Lewis and Outcalt 1976). That study used an airplane-mounted sensor, but technology has improved significantly since that time. In fact, it is now possible to obtain thermal information for huge areas of the Earth with great regularity, consistency and affordability because satellites in orbit continuously gather it. These improvements are reflected in another UHI study in the 1980s when Dousset and Gourmelon (1986) demonstrated UHI patterns for Los Angeles and Paris using thermal imagery from the National Oceanic and Atmospheric Administration's Advanced Very High Resolution Radiometer (NOAA AVHRR) satellite system. That study also utilized imagery gathered from the SPOT satellite to analyze the influences that various land covers in those cities were having on the UHI patterns, especially with regards to how vegetation was affecting them. Even so, these remotely sensed data come with their own limitations. First of all, the satellite imagery is only available for the time when the recorders are orbiting above an area which normally occurs on the order of once every sixteen days, depending on the sensor. In addition, atmospheric and weather interference like clouds may impact the usability of the remotely sensed data. There are also problems associated with the nature of what the satellites are recording that present concerns of their own. The satellites are not recording actual temperatures, but are instead recording energy in the infrared part of the electromagnetic spectrum that is being emitted from objects on the surface as it rises to the top of the atmosphere. These

radiance values can be converted into brightness or blackbody temperatures using Plank's Law (Dash, et al. 2002). But these brightness temperatures differ from the true (kinetic) temperature of the surface by a factor that depends on the emissivity of the surface, so conversion of the satellite radiance into true temperature requires knowledge of the surface optical properties. Even after those factors are taken into account, there are still complications which cannot be ignored when working with thermal infrared satellite data. Thermal radiation emission rates vary widely between surface types, vegetation types, soil types, and moisture levels. Because urban areas contain a myriad of surface and material types which all emit IR energy at different rates, the amount of IR energy emitted can vary widely over small areas as well as temporally (Arnfield 2003). Further complicating matters, these space mounted instruments are not collecting data from vertical surfaces like walls which are elementary parts of urban environments.

Besides the problems associated with emissivity variability, there are atmospheric effects which can complicate the IR readings. The energy passes through many different types of gases which are also quite variable in the atmosphere, so atmospheric corrections must also be made when using remotely sensed thermal data. One UHI study for the city of Rome was done partly to test the accuracy of established algorithms which attempted to convert values recorded by satellites to actual air temperatures, and found them to have serious shortfalls (Fabrizi 2010). While that particular study was successful in its goal of developing a better conversion algorithm, its results may not be directly transferrable to other places or situations without further amendments. Another important aspect of the Fabrizi study was the mixed approach, in which a combination of remotely sensed data and in situ ground air temperatures were combined.

In addition to those complications, there are other issues which limit the use of thermal data obtained by aircraft and satellites. The spatial resolution is often poor compared to other spectral bands such as visible light. Because thermal wavelengths are much longer, they carry less electromagnetic energy and so to compensate, thermal infrared energy is normally collected from a larger ground cell resulting in lower spatial resolution. Specifically, LANDSAT ETM produces imagery with a spatial resolution of 30 X 30 meters in the visible light wavelengths, but thermal band imagery has a 60 X 60 meter pixel size (Jensen 2007). Airplane mounted cameras and imagery with much finer resolution is available, but the costs of obtaining such data are extremely high. Additionally, the methods for converting remotely sensed urban land surface temperatures into actual air temperatures are not always easily done with great accuracy (Fabrizi 2010).

One shortfall in satellite data for urban microclimate studies is imagery timing. LANDSAT ETM, a very popular source of satellite imagery, and most other satellites pass over the United States at times which are not optimal for UHI studies. They usually pass over early in the morning before maximum heating of land surfaces occur, and at night when heat island effects may have degenerated (Weng 2009).

Even so, remotely sensed data from airplanes can provide improved spatial resolution for infrared imagery and has been used in UHI studies with great success. While it is more expensive than satellite imagery, Gluch et al. (2005) used airborne thermal data with a ten meter spatial resolution to document the UHI effect in Salt Lake City, Utah. That study linked thermal patterns to land use and cover types of surfaces, and quantified how much surface temperatures differed depending on land use and cover.

Because UHI is generated by complex urban surfaces which vary greatly in size and shape, understanding these interactions on even smaller scales will be beneficial if problems associated with them are to be addressed. It is at these scales which people experience their environments. These processes are extremely complicated at small scales and are very difficult to model accurately at this time. Even so, there are studies which address smaller scales seeking specific contributions to UHIs from various urban surfaces and land cover types. Huang, et al. (2008) documented air temperature differences related to urban surface types in the city of Nanjing, China successfully using a multi-scaled approach. That study demonstrated diurnal temperature changes for several kinds of surface features which are common to all cities and their findings should be applicable to many other cities which experience UHI effects.

2.4 Integrating Data and Methods, GIS

Combining satellite imagery with other data sets to assess UHI patterns and impacts is now very common, especially with the development of Geographic Information Systems (GIS). Perhaps the most common approach utilizes the Normalized Difference Vegetation Index, NDVI (a measure of vegetation density), to predict UHI intensity (Weng 2009). Because vegetation can greatly inhibit the development of UHIs, this approach compares the amount of vegetation to the amount of land covered by impervious surfaces and is often very helpful at displaying UHI patterns when applied to urban thermal studies. This combination will likely remain a valuable tool for UHI studies in the future.

2.5 Additional Environmental Features

Because buildings are the main features of urbanized areas, their design and impacts often affect areas in their immediate proximities. Sometimes they have effects which are unintended and quite severe. One excellent example of a building generating excessive heat occurred in downtown Los Angeles at the newly built Disney Hall, designed by Frank Gehry in 2004. The building is not traditionally shaped, but instead includes a variety of curves and reflecting surfaces. This has resulted in solar energy being concentrated and refocused towards nearby residential buildings and increased temperatures in them by as much as 8° C (15° F). After neighbors complained, some reflective surfaces were dulled to remedy the uncomfortable impacts on adjacent properties (BBC News 2004). While this may be an extreme example, it does demonstrate how localized microclimates may be impacted by nearby structures.

Since UHI impacts affect energy use in buildings, there are numerous studies surrounding "smart" and "green" buildings. One such study by Oberndorfer et al. (2007) found great benefits when replacing traditional rooftops with plantings and vegetation cover (so called "green roofs"). Some of the benefits included better storm water management, lowered cooling and heating costs, increased ecological functioning and wildlife habitat, in addition to reducing UHI effects. There is a great deal of overlap between architectural studies, sustainability studies, and urban climate/UHI studies. Increasing vegetation cover helps to reduce UHIs significantly.

Vegetation is one of the features which most successfully mitigates UHI effects. The loss of vegetation is one of the primary causes of UHIs in the first place. Trees offer

a very good example of how vegetation's mitigating factors work. For example, trees shade areas beneath them from sunlight, which reduces solar heating. They also help cool the air around them by the evaporation of water through their leaves during transpiration (Akbari, Pomerantz and Taha 2001). In fact, shading by trees has been proven so beneficial that many progressive cities in California have implemented ordinances calling for shade trees to cover as much as fifty percent of parking lots (McPherson 2002). This report, also published by UC Davis, proved that even modest shading of parking lots by trees resulted in enough cooling to greatly decrease gasoline evaporation from parked cars, and that those reductions would lead to measureable improvements in air quality over time.

Another important factor in studying the UHI phenomenon is called the "sky view" factor. Sky view factor is a measurement of the amount of visible sky from any particular point. In cities, the main features which block the sky view are buildings and walls as well as trees. Because outgoing long wave radiation that leads to cooling may be impaired by features which block its dispersion into the open air, these parameters are increasingly being fed into models for UHI studies. While there have been some conflicting findings due to differences in methodologies, urban geometry's effects on the sky view factors has been shown to significantly affect air temperatures (Unger 2009) in some studies. For that reason, future UHI studies will likely include this factor when applicable.

2.6 Computer Modeling

Most atmospheric heating occurs when air comes into contact with a sun-warmed surface. Energy flux studies on how heat is transferred from objects into that air above them are extremely complicated for urban areas because so many different kinds of surfaces are present (Gluch, Quattrochi and Luvall 2005). Even so, some mathematical models have been used which are increasingly successful at smaller scales such as those found in urban canyons (the areas of street and sidewalk between buildings in city blocks) and the built environments that we inhabit. For example, in 1998 Bruse and Fleer performed a study of the interactions between surfaces, plants, and the air in a simulated urban area. The findings of that study showed that relatively small changes in urban settings can have large changes in microclimate features over small areas. Their findings also indicated that the temporal elements of heat flow between urban features and the environment greatly increased the complexity of their models. Bruse and Fleer finished by stating the need for more numerical and computer studies on urban climate effects to help optimize our urban living environments in the future (1998).

Unlike the previously mentioned systems, these approaches can be very useful at micro-scale simulations. One such program, called “ENVI-met” was used by Heldens et al. (2010) to map a small area of a German town. While it was quite reliable at predicting what air temperatures would be in that setting, that approach has its limitations. Air temperatures are affected by many kinds of variables, from solar energy, cloud cover, humidity, wind direction and speed, to the heat capacities and other data about specific surfaces. Some of those data are readily obtainable while others are not yet widely available for the public. Another European study focused on a single urban canyon area

and quantified the effects of urban geometry and building materials on the microclimate in Kassel, Germany in 2008. That model was very detailed, but only covered a very concentrated area of the city. Even so, it provided useful information for urban planners in that area when studying ways to reduce possible potential impacts caused by a warming climate (Katzschner and Thorsson 2009). These models are informative; however, they are not easily converted into city-wide scales despite a tremendous increase in the number and variety of these studies since their inception (Arnfield 2003).

2.7 Improvements in Data Collection Devices

In recent years, air temperature recorders have become more widely available and less costly, so detailed temperature mapping is much more feasible than it has been historically. These devices can greatly improve our understanding of some of the ways in which our built environment is affecting temperature patterns in our daily lives. In doing so, these devices can also help us clearly understand our urbanized environment's thermal patterns so that planning for our cities can be improved. While there are numerous examples of UHI studies that use many different approaches, there are relatively few that have used dense networks of temperature data loggers. One problem is protecting such devices from theft and vandalism while embedding them in an urban setting. In any case, the data sets generated by dense networks of temperature loggers would prove useful in urban studies and also help determine the accuracy of computer simulations done for the same areas.

3 Methodology

3.1 Study Area

The study area for this project is the campus of California State University, Northridge. It is located in the San Fernando Valley and the city of Los Angeles, California. Northridge has a Mediterranean climate which is characterized by cool, wet winters, and warm to hot, dry summers. The average high temperature during the month of July in Northridge is 35° C (95° F). The average low temperature is 13.9° C (57° F). July is the second warmest month in this area and it is the driest month on average with precipitation only averaging 0.5 millimeters annually (The Weather Channel 2012).

It is a heavily urbanized region but not as densely urbanized as the downtown Los Angeles area. Even though the development is less dense, there are many types of surfaces on campus associated with UHI effects: large buildings, parking lots, streets, and sidewalks. There are also many surfaces on campus known to moderate or reduce UHI effects: trees, shrubs, and irrigated lawn areas. The campus was chosen for this study because it incorporates both the features of planned parkland areas with commercial development commonly found in modern cities. It is a large property that is under the control of a single entity, and while open to the public, its public use is limited compared to parks, commercial, and residential areas. In an attempt to reduce tampering or theft of sensors, residential areas of campus were excluded. For that reason, this study does not include the entire campus, but instead consists of the southern portion, bounded by Nordhoff Street on the south, Darby Avenue on the west, Halstead Street on the north

(approximately) and Zelzah Avenue on the eastern end. Figure 2 displays the study area as well as its location in Southern California

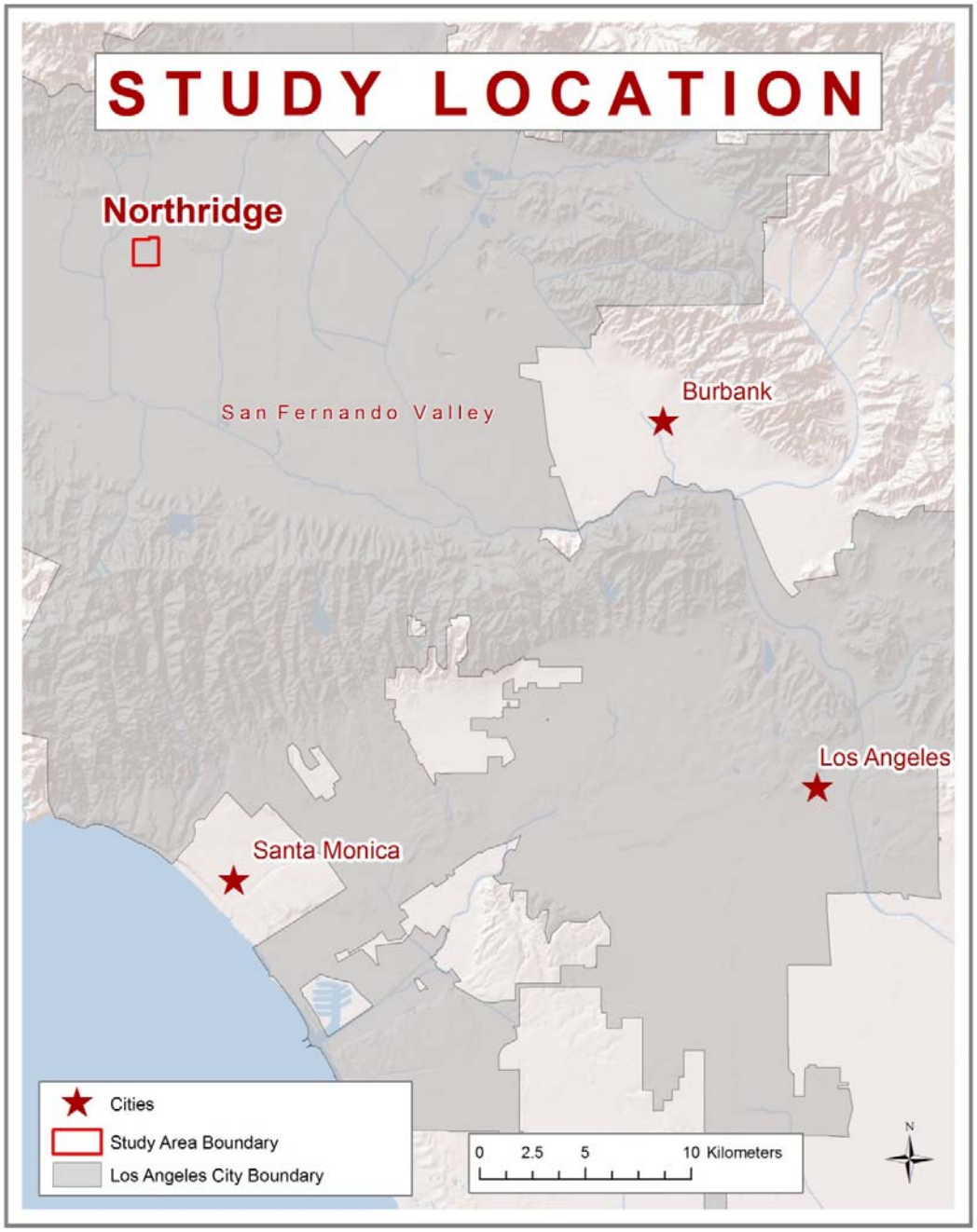

Figure 2. Northridge is north and west of downtown Los Angeles.

3.2 Data

An orthorectified aerial image was obtained for the study site in order to provide a clear, two-dimensional depiction of the campus. It consisted of four bands, representing the red, green, blue, and near infrared portions of the electromagnetic spectrum. The date of the imagery was March 10, 2012 and the resolution was one foot per pixel. It was a GeoTiff format and had a State Plane Projection (Region 5) using the North American Datum 1983 coordinate system. This served as the base imagery for the project.

Air temperature data were recorded using Thermocron 1-Wire/iButton Part Number: DS1921H-F5 sensor/loggers sold by the Maxim Integrated Company. These micro-processor sensors were encapsulated in small camera-battery sized stainless steel capsules (17.35 MM X 5.89MM) capable of measuring and recording temperature data at user defined rates between 1 and 255 minutes. Each logger has an SVRAM memory which allows for storage of up to 2048 different values. The accuracy is +/- 1 degree Celsius and resolution is .125 degrees Celsius. Their ideal operation temperature range is between 15 and 46 degrees Celsius and each logger contains a real time clock.

The sensors were programmed to record temperature data hourly concurrently and those values were later downloaded into Microsoft Excel as a comma separated value (CSV) format. Each sensor provided its own Excel data table which then had a sensor number value appended to it; those tables were later joined into a single Excel table and converted to an .xls file format and then imported into ArcMap GIS software.

3.3 Placement of Sensors

One hundred and two sensors were deployed around the CSUN campus on July 1, 2012. Sites were chosen using aerial imagery to obtain samples of the main types of surfaces and landscape types most common on campus. Large homogenous areas were most desirable, but one major limiting factor was the existence of appropriate mounting structures. Trees were the most common mounting structures since they were most readily available and offered some protection from direct solar radiation at the hottest times of the day. Other features that were utilized to affix the sensors were light posts and steel beams used to hold up solar panels. All sensors were mounted with shading from direct solar radiation provided via a custom made aluminum foil solar shield. When a surface other than wood was used for mounting, a three inch piece of foam was used with Styrofoam spacers to prevent heat transfer from the poles to the sensors. Walls and buildings were avoided as mounting places. The sensors were removed on July 16th, 2013.

3.4 Data Processing

Upon collection, the temperature data from each sensor were compiled into a single spreadsheet. Hourly data were then averaged across all sensors and the standard deviations calculated. Outliers were identified by finding those readings which exceeded three standard deviations for any hour's data. Positive outliers were most often associated with damaged solar shields, or sensors that appeared to have been tampered with in some way during their deployment. Those sensors were excluded from the study. Some sensors recorded abnormally low temperatures at some points during the study.

These only occurred in areas known to be heavily irrigated. The most likely cause was that the sensors were wet for short periods. When negative outliers only occurred for durations of less than two hours and did not exceed more than five instances for any sensor, null values replaced those abnormally low temperatures so that the effects of wet sensors would not impact later analyses. There were thirty instances in which this process was applied. Of the 102 sensors deployed, only 93 provided data that were used in the analysis. With each sensor recording hourly for two weeks, the final spreadsheet contained a total of 31,218 temperature records.

3.5 GIS and Group Classifications

As sensors were deployed, their locations were recorded using a global positioning system (GPS) device. Those sensor locations were then plotted in a GIS and minor adjustments were made against the aerial imagery to correct for insufficient GPS accuracy. Using GIS, a ten meter buffer was created around each sensor location. Areas in the vicinities of sensors were digitized as impervious or permeable surface types using the aerial imagery. This allowed for calculations of how much area within ten meters of each sensor was covered by impervious surfaces. In places where the imagery was difficult to interpret, field measurements of surface type and their dimensions were recorded on site.

Once the percentage of impervious surface cover within ten meters of each sensor was calculated, the sensors were separated into four groups. General characteristics of the four groups are as follows:

A- (0 – 25% impervious) predominantly lawn or other permeable surfaces, usually covered with irrigated vegetation. (28 sensors)

B- (26 – 50 % impervious) less permeable surface area, but still mostly permeable and some vegetation. (19 sensors)

C- (51- 75 % impervious) a combination of lawn or other ground covers but more concrete or asphalt, with less vegetation. (22 sensors)

D- (76-100 % impervious) mostly cements and asphalt ground coverings with little or no vegetation. (24 sensors)

Figure 3 shows parts of the digitizing layers used in classifying each sensor location. The background is a close up of part of the imagery. The yellow features represent the step of separating impervious from permeable surface types. The pink points show some of the sensor locations. The orange circles are the ten meter radii which were used in combination with the yellow layer to calculate the percentages of impervious surface area for each sensor. Figure 4 is a map showing the sensor locations and their assigned classifications of A, B, C, or D. It also shows the locations where sensors were deployed but were damaged or lost while collecting data.

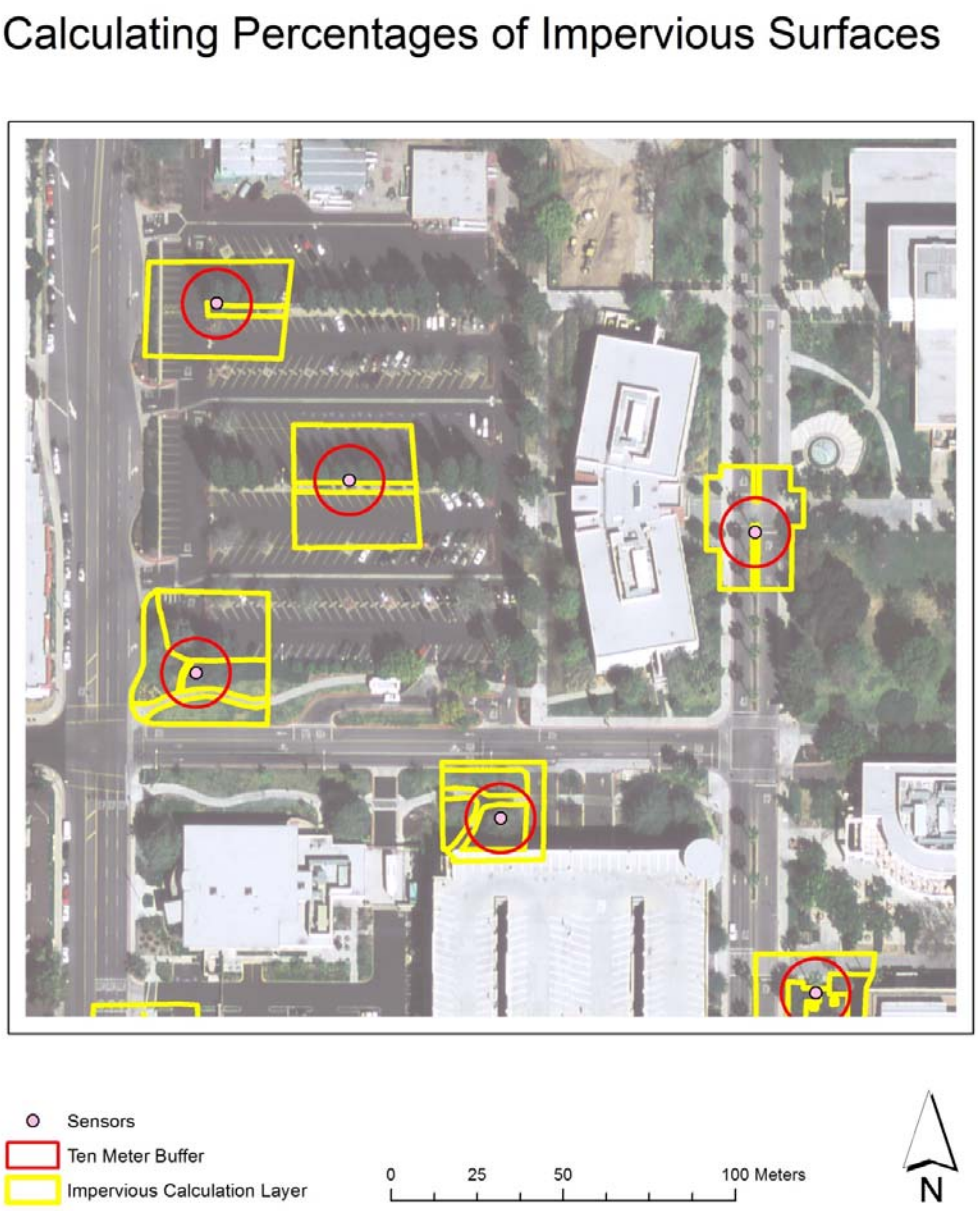

Figure 3. Impervious and permeable surfaces surrounding each sensor were digitized using the base map imagery. The sensor locations were then buffered by ten meters. Calculations were then made using the impervious calculation layer that fell within the buffers so that each sensor could be classified into their respective groups.

Sensor Locations

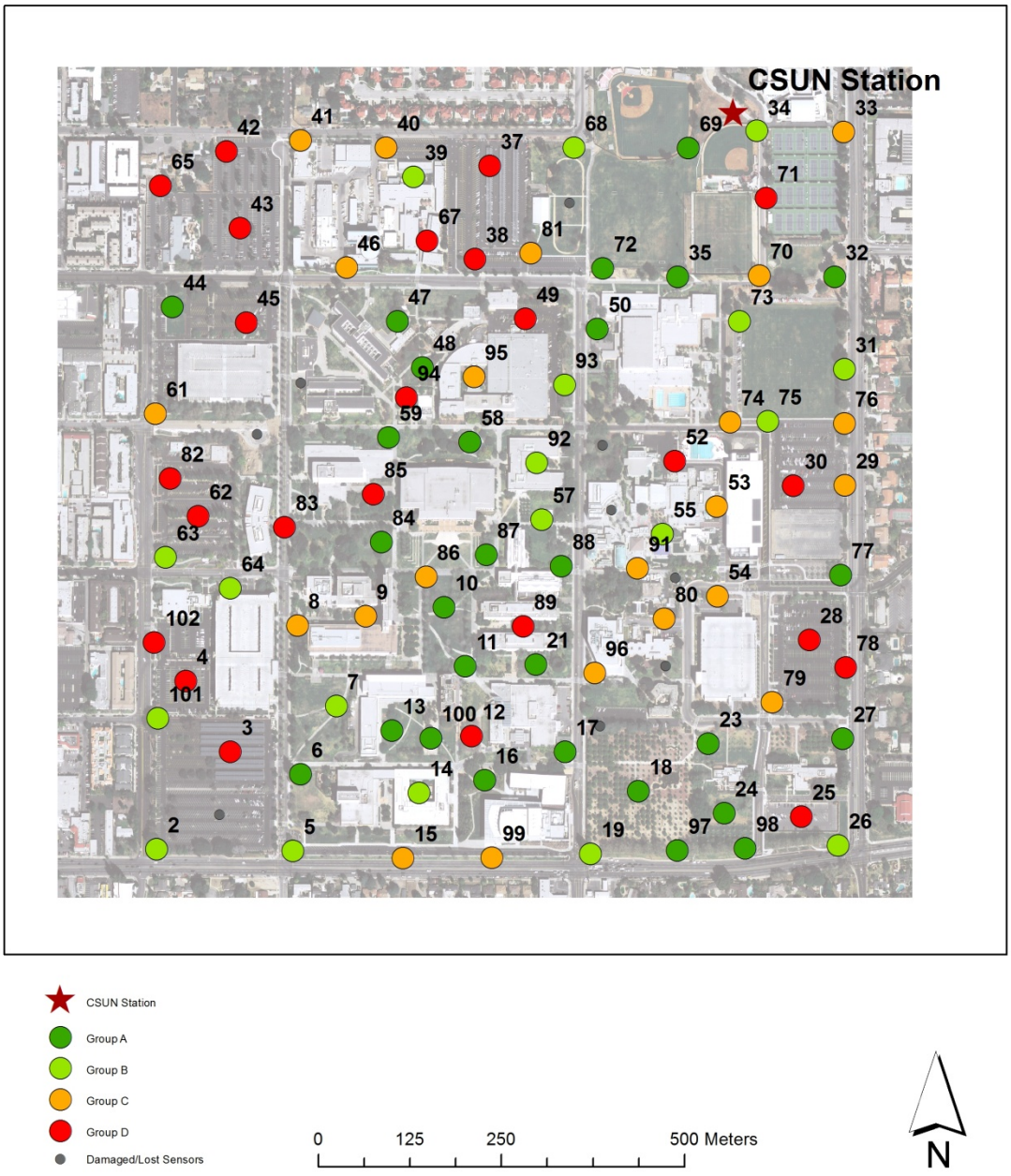

Figure 4. The locations of each sensor as well as the classes into which they were assigned. Note the locations of sensors which were lost or damaged.

3.6 Datasets Analyzed

After the data were collected and imported into a spreadsheet, several data sets were extracted for use in further analyses. The first analysis was performed on the mean temperature data from the entire duration of the study. After that, the average high and low temperatures were examined. Next, the average temperatures at each hour were calculated so that temporal analyses were possible. Because July 10th was the warmest day and 4:00 PM was warmest hour, the data for that hour were examined. Finally, because UHIs are most common in the evening hours during hot weather, the hours following sunset on that hottest day were analyzed to see if UHI patterns occurred.

3.7 Mapping Temperatures and Statistical Analyses

The first task for each data set was the creation of an inverse distance weighted raster (IDW) so that a temperature pattern using the data could be displayed. This technique uses the temperatures at each sensor location and estimates temperatures at all places between these. The sensors closest to any unknown values affect the interpolated values much more strongly than more distant ones. The form of the algorithm used in IDW interpolation is as follows:

$$F(x,y) = \sum_{i=1}^{n} w_i f_i$$

where *F(x,y)* is the assigned value for the interpolated cell, f_i are the temperature values at the sensor locations, *n* is the number of sensors, and w_i is the weight (or influence) of sensor *i* at the interpolated cell *(x,y)*.

The weights, w_i, are defined as:

$$w_i = \frac{d_i^{-p}}{\sum_{j=1}^{n} d_j^{-p}}$$

where p is a real number called the power parameter, usually 2, and d_i is the distance from sensor i to the data point being estimated. A value of 2 for p results in the inverse distance squared interpolation ("inverse square law"); this was the value used in this application. The effect of sensor temperatures on estimated values decreases with increased distance from a sensor; the higher the value of p, the more rapid the decrease. The distance, d_i of a point (x,y) from sensor i at (x_i,y_i) is given by:

$$d_i = \sqrt{(x - x_i)^2 + (y - y_i)^2}$$

The result was an image which displayed those estimated temperature values over the entire study area. A classification was assigned to the temperature values so that cooler areas appeared blue. With increases in the estimated temperatures, the colors changed from blue to yellow, orange and red as temperatures rose. This change allowed for a visual inspection of where the warmer and cooler temperatures were for any data set examined but no statistical analyses were performed on those estimated temperatures.

There were two kinds of statistical analyses performed on the data. The first analysis examined the relationship between the percentage of impervious surface cover within ten meter radii of sensors and air temperatures recorded. For that test, the data were graphed in scatter plots with the percentage of impervious cover variable on the x axis and the measured air temperatures on the y axis. Computer assisted correlation analyses were performed which resulted in Pearson's product-moment coefficients. The

end results of those tests were *r* values between -1 and 1. The data were positively correlated because all of the *r* values were positive. The interpretation guidelines for the *r* values were as follows:

- 0.9 – 1.0 very strong
- 0.7– 0.89 strong
- 0.5 – 0.69 moderate
- 0.3– 0.49 moderate to low
- 0.16– 0.29 weak to low
- Below 0.16 too low to be meaningful

After the correlation analyses were performed, the data were grouped into their respective groupings for the second type of statistical analyses.

I. Analysis of group averages graphed using bar charts.

II. Box plots graphing variations within groups and comparing group medians.

Once those charts were generated, comparison of means statistical analyses were employed to determine whether or not each group's average indicated that the data came from statistically distinct populations, or fell within the ranges which were possible due to sampling variations and hence were not likely discernible as distinctly separate groups. For that kind of analysis, a Kruskall-Wallis one-way analysis of variance test was used for comparing means between groups. That test measures the variation within each group as well as the amount of variation in all of the data to assess whether at least one of the four groups was statistically distinct from the others. A significance level of .05 was

used for those analyses. When statistical differences were classified as likely, Mann-Whitney U tests were used to determine which group(s) differed from others. Once again, a confidence interval of .05 was used when interpreting the *p* values from those tests. The results of those tests were summarized and for the temporal analyses, listed in a table showing which groups were statistically distinct or statistically indistinguishable from the other groups.

3.8 CSUN Weather Data

CSUN operates a weather station which is located near the northern end of the study area. The station collects data on precipitation, humidity, solar radiation, barometric pressure, wind speed and direction as well as air temperature data. The weather during the study, from July 2, 2012 to July 15, 2012 was typical for the time of year. There was no precipitation recorded, days were mostly sunny and winds were generally light averaging less than three miles per hour. The warmest temperature was 38.89° C (102° F) and occurred on July 10th. The coolest temperature was 13.72° C (56.7° F) on July 8th. The data obtained by the CSUN weather station were not included in the calculations for this study; however, they are included with some of the charts for comparison with data obtained by the study's sensors. A graph of the minimum and maximum temperatures recorded by the weather station follows in figure 5.

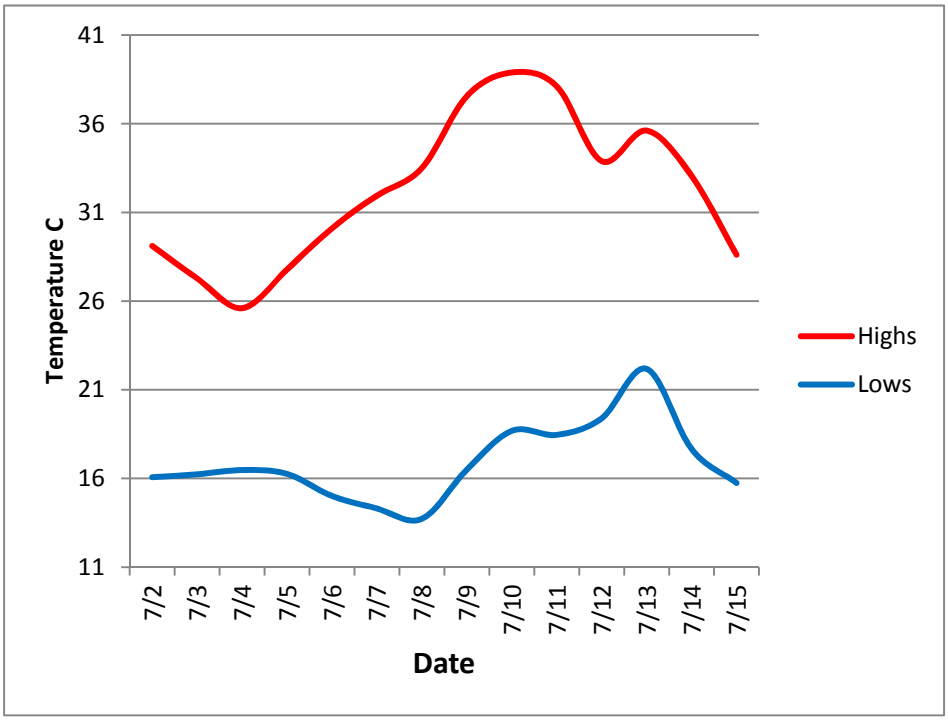

Figure 5. The maximum and minimum temperatures recorded each day during the study by the CSUN weather station.

3.9 Surface Temperature Data

Surface temperature data were recorded at several times during the study using a battery operated, digital, infrared thermometer. Those data were not statistically analyzed or mapped in this study but are referred to as contextual data in some cases when discussing differences in air temperatures likely driven by those actual surface temperatures.

4 Results

4.1 Mean Temperatures

The average temperature from all of the sensors taken over the entire duration of the study was 24.37° C (75.86° F). The highest average temperature for any individual sensor was 25.71° C (78.28° F) recorded by sensor #85 (Group D). That was 1.35° C above the mean. Sensor # 97 (Group A) recorded the lowest average temperature of 22.74° C (72.93° F). That sensor's average temperature, the coolest recorded, was 1.63° C below the overall mean. Thus the difference between the average temperature recorded by the hottest and coolest sensors was 2.97° C.

Figure 6 shows the IDW raster created using the mean temperature from each sensor. There is a noticeable pattern of warmer temperatures along the western and eastern sides of campus. These areas of warmth coincide with highly impervious features, specifically parking lots, which are found mainly in those areas. The cooler regions were found in more central areas where large expanses are grass covered and less area is covered by impervious surfaces. The range between the coldest and hottest mean temperature values of 2.97° C is consistent with findings from another UHI study carried out by Huang, et al. (2006) which found UHI intensity varying between 0.5° and 3.5° C. Among the averaged data sets analyzed (mean temps, average highs, and average lows) this mean temperature data displayed the highest correlation coefficient using a Person product-moment correlation test.

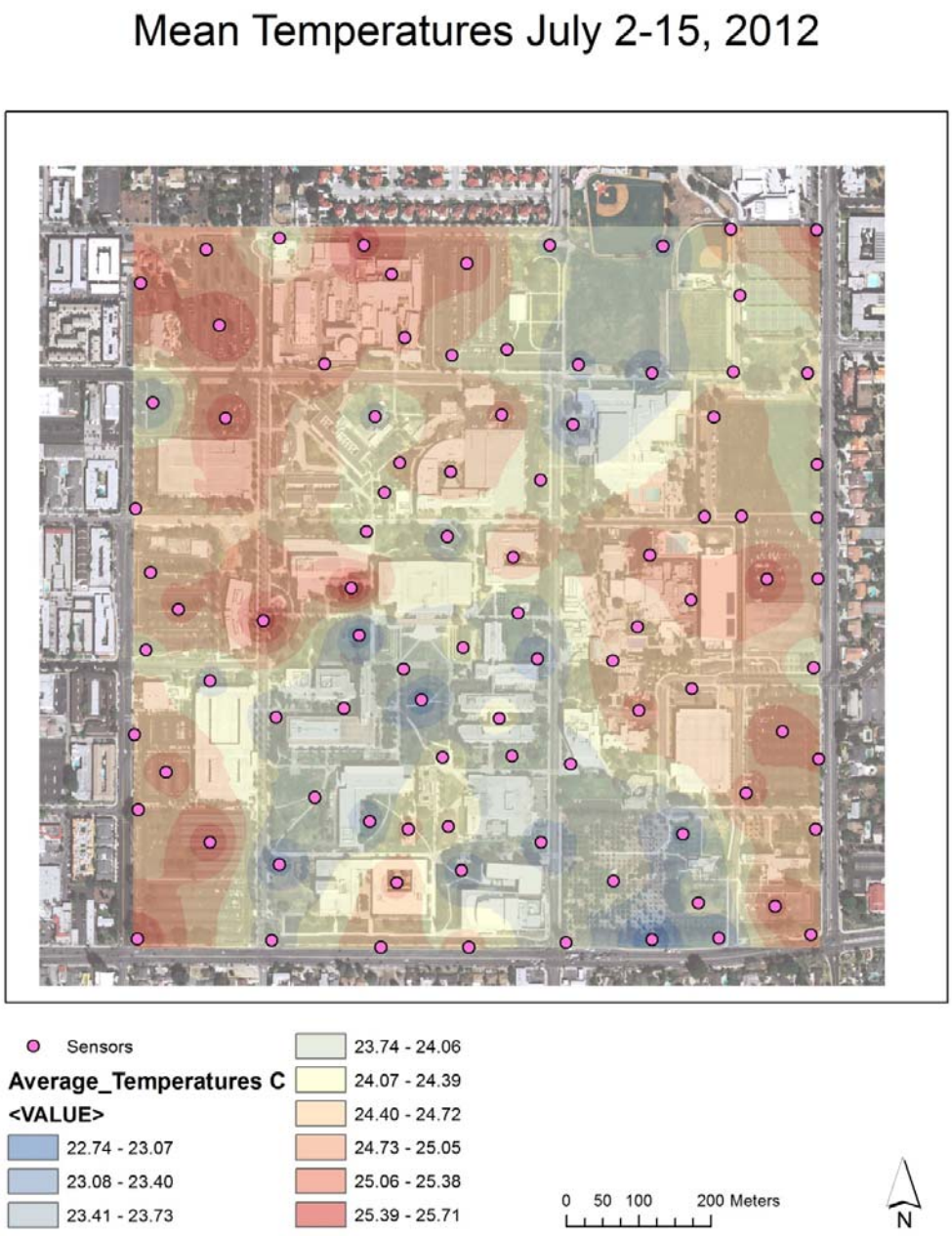

Figure 6. An IDW raster created by using the exact mean temperature values provided by the sensors and estimating temperatures in between them based on distance from known values.

The mean temperature data were plotted and analyzed to determine if there was a relationship between the percentage of impervious surface cover around sensors and the mean air temperatures recorded over the study period. A Pearson product-moment correlation coefficient was computed to assess the strength and direction of that relationship. The results of that test (r^2=0.533, r=.73, n= 93, p=.000) indicated that a strong positive correlation exists between those variables (r=.73). The r^2 value of .533 means that roughly 53% of the variation in the mean temperatures can be explained by differences in the percentage of impervious surface cover near the sensors. There were 93 samples used in the calculation (*n)* and the *p* value of less than .001 indicates a high confidence level in this finding. Figure 7 summarizes those results.

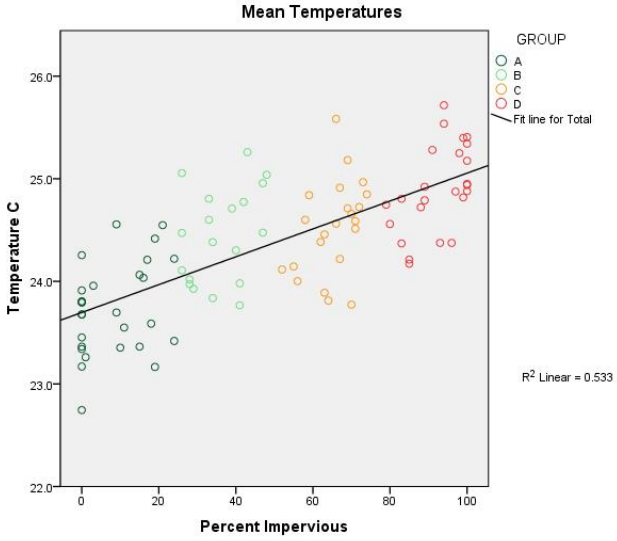

Figure 7. A scatter plot showing the mean temperatures against the percentage of impervious surface cover surrounding the sensor locations. The Pearson's r correlation coefficient was .73, which is considered a strong positive correlation.

The average temperatures for each group were then calculated. Group A had the lowest average temperature which was 23.73° C (74.71° F). Group B's average temperature was 24.44° C (75.99° F). The average temperature of Group C was 24.52° C (76.13° F). Group D's average temperature was 24.9° C (76.82° F). There was a difference of 1.17° C between the warmest and the coolest averaged group temperatures. That data is displayed in figure 8.

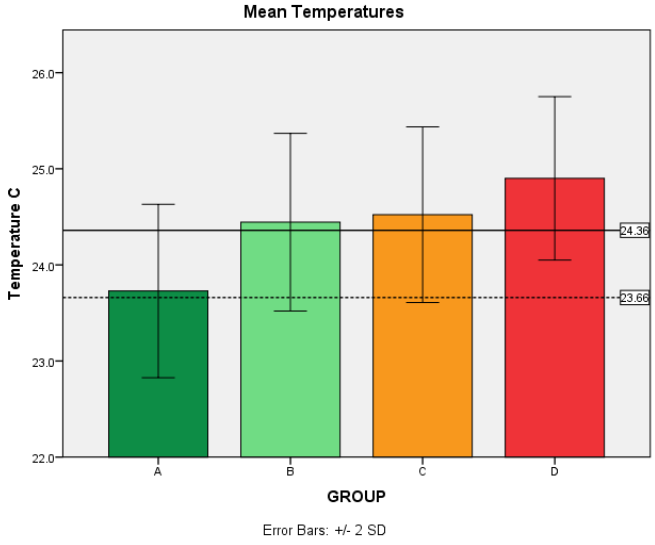

Figure 8. The grouped mean temperature data along with vertical bars representing two standard deviations from those means. The solid black line displays the mean temperature from all of the sensors. The dashed line displays the mean temperature recorded at the CSUN weather station during the study period.

When the average temperature of each group was subtracted from the mean temperature of all the observations (24.36° C; 75.8° F), the group average that was the most distant from the overall mean temperature was Group A. That distance was 0.64° C below the mean. The Group B average was closest to the mean, exceeding it by 0.08° C. Group C exceeded the mean by 0.16° C. The average from the sensors comprising Group

D exceeded the mean temperature by 0.54° C. The range of values between the highest and the lowest grouped average was 1.17° C.

The CSUN station recorded an average temperature of 23.66° C (74.59° F) during that same period, which is 0.7° C cooler than the overall average from all the sensors. The surface features surrounding that station would place that sensor into Group A and Group A's mean temperature of 23.73° C (74.71° F) differed by only 0.07° C from that CSUN weather station's 23.66° C (74.59° F).

Figure 9 is a box plot chart that displays the median value of the grouped mean temperatures and the distribution of the data points around each group's median. The colored boxes represent the 50^{th} percentile range around the medians. The "whiskers" above and below the boxes represent the minimum and maximum values in each group. The median of the averaged temperatures was 24.38° C (75.88° F) and is represented by the solid black line in the chart. The Group A median is clearly lower than the other groups.

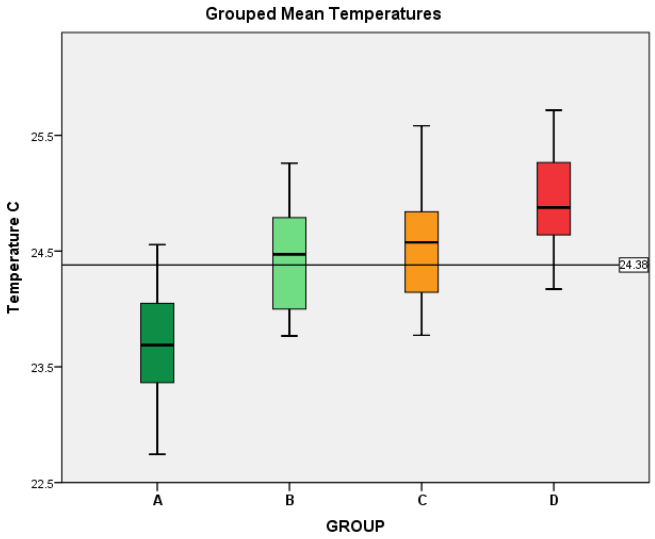

Figure 9. A box plot graph comparing the medians of the mean temperatures separated into their respective groups. The solid line represents the median temperature from the sensors. The dark lines inside the colored boxes lie at the medians for those groups.

Group A's median was 23.68° C (74.62° F). There was a 1.81° C difference between the hottest and coldest sensor in that group. That range was tied with Group C for the number of degrees separating the hottest and coldest sensor. Group B had the smallest range amongst its sensors of all the groups. That range was 1.49° C and the median value was 24.47° C (76.15° F). Group C's median was 24.57° C (76.22° F). The Group D median was 24.87° C (76.77° F) with a range of 1.54° C. The differences in the standard deviations was negligible, ranging from 0.42 (Group D) to 0.46 (Group B). These data are summarized in table 1.

Table 1. Descriptive statistics from the grouped mean temperatures data.

Group	Mean	Median	Std. Dev.	Min.	Max.	Range	Dep. Avg.
A	23.72	23.68	0.45	22.74	24.55	1.81	-0.64
B	24.44	24.47	0.46	23.76	25.25	1.49	0.08
C	24.52	24.57	0.45	23.77	25.58	1.81	0.16
D	24.90	24.87	0.42	24.17	25.71	1.54	0.54

The results of the Kruskall-Wallis test on the grouped mean data indicated that there was a significant difference between at least one of the groups (p-value < .001). Groups were then paired and the Mann-Whitney U tests were conducted to see which groups differed significantly among the four. Group A was paired against Group B and the resulting p-value of less than .001 indicated that the difference between those two groups was significant. Group B and C were compared and the resulting p-value of .619 indicated that these two groups were not significantly different from each other. Comparing groups C and D resulted in a p-value of .009 so those groups also differed significantly.

The results of these tests indicated that a total of three statistically distinct populations were present in the data. One group was comprised of Group A, which was statistically cooler. Groups B and C comprised a group of intermediate mean temperatures, while Group D also stood apart as statistically warmer. These mean

temperature data exhibit a general UHI pattern with the extremely permeable surface areas as cooler and the most impervious areas warmer. It also demonstrates the difficulty of predicting UHI effects in areas of great surface heterogeneity, as in the middle (combined) groups (B and C).

4.2 Average High Temperatures

The mean daily high temperature from all of the sensors over the duration of the study was 32.99° C (91.38° F). This was 0.77° C warmer than the average daily high temperature recorded at the CSUN weather station, which was 32.21° C (89.98° F). The sensor with the lowest averaged daily high temperature was #97 (Group A). That sensor's averaged daily high temperature was 30.34° C (86.61° F), which is 2.65° C below the mean. The sensor recording the highest averaged daily high temperature was #53 (Group C). Sensor #53 averaged 35.7° C (96.26° F) which was 2.7° C above the mean. The difference between the highest and lowest averaged daily high temperatures was 5.36° C.

Figure 10 is an IDW raster produced using the averages of the daily high temperatures. Again, the warmer areas are located along the east and west peripheries of campus with the cooler areas found towards the center of campus. The 5.36° C temperature difference in average high temperatures between the coldest and hottest sensors are consistent with conclusions reached by Taha (1997) which found that changes in albedo, if employed by cities, along with increasing vegetation, could reduce air temperatures by up to 6° C in some instances.

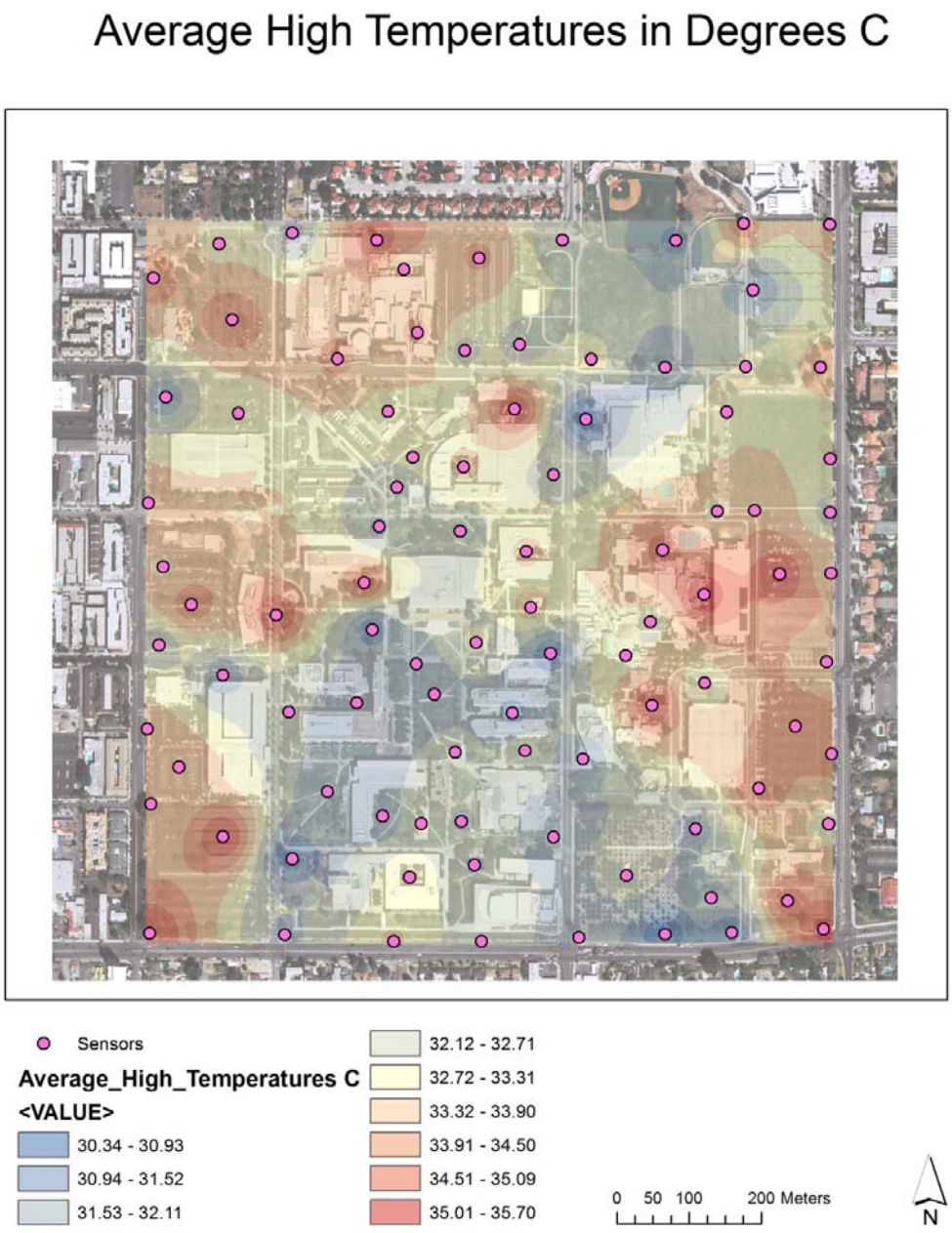

Figure 10. An IDW raster created by using the averages of the daily high temperatures and estimating temperatures in between them based on distance from known values.

The average high temperature data were plotted and analyzed to determine if there was a relationship between the percentage of impervious surface cover near sensors and the average high temperatures recorded over the study period. A Pearson product-moment correlation coefficient was computed to assess the strength and direction of that relationship. The results of that test (r^2=.324, r=.56, n= 93, p=.000) indicated that a moderately positive correlation exists between those variables (r=.56). The r^2 value of .324 means that roughly 32% of the variation in the average high temperatures can be explained by differences in the percentage of impervious surface cover near the sensors. The p value of less than .001 indicates a high confidence level in this finding and there were 93 samples used in the calculation (n). Figure 11 below summarizes those results.

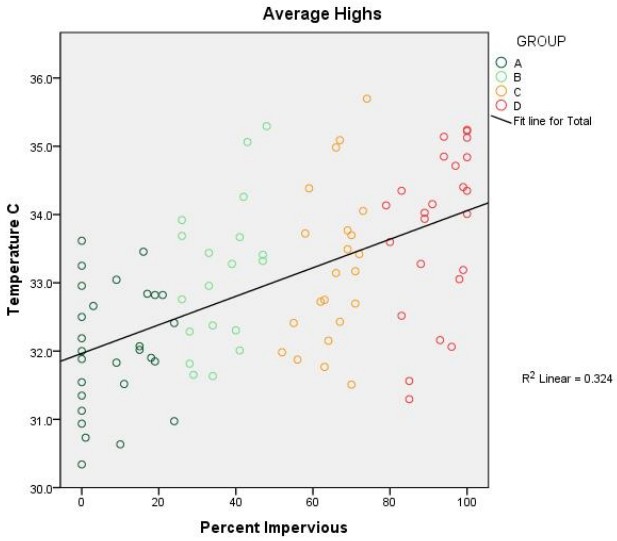

Figure 11. A scatter plot showing the average high temperatures against the percentage of impervious cover surrounding the sensor locations. The Pearson's r correlation coefficient was .56, which is considered a positive correlation of moderate strength.

The average of the daily high temperatures was 32.99° C (91.38° F). The CSUN weather station's average high was 32.21° C (99.99 ° F) a difference of 0.78° C. The average high temperature for Group A was 32.04° C (89.67° F) and that was the lowest as well as the most distant from the mean (-0.95° C). Group B's average daily high was 33.11° C (91.60° F); that was 0.12° C above the mean. Group C's average was 33.22° C (91.80° F) and was 0.23° C above the mean. Group D's average was 33.8° C (92.84° F), the warmest group was 0.08°C above the mean. The difference between the warmest and the coolest grouped average highs was 1.76° C. Those values are graphed in figure 12.

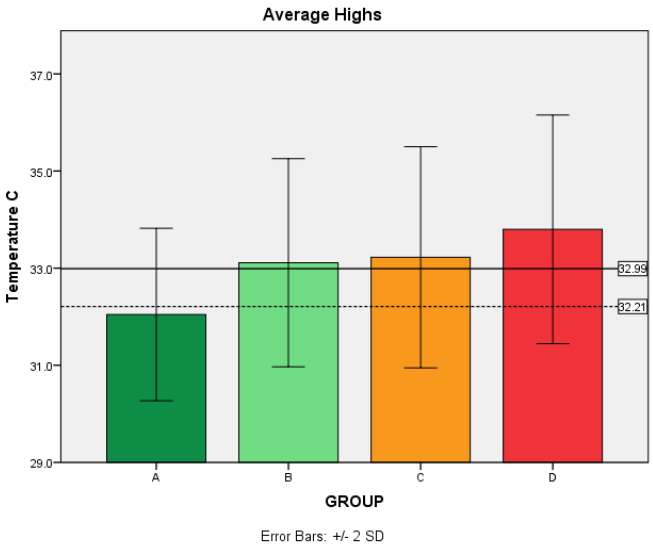

Figure 12. The grouped average high temperature data along with vertical bars representing two standard deviations from those averages. The solid black line displays the mean temperature from all of the sensors. The dashed line displays the mean temperature recorded at the CSUN weather station during the study period.

Figure 13 is a box plot chart which displays how the grouped averaged daily high temperatures varied around the median values. The median of the averaged daily high temperatures was 32.96° C (91.33° F) and is represented by the solid black line in the chart. The Group A and Group D medians stand visibly apart from the medians of Groups B and C, which display a significant amount of overlap in temperature ranges.

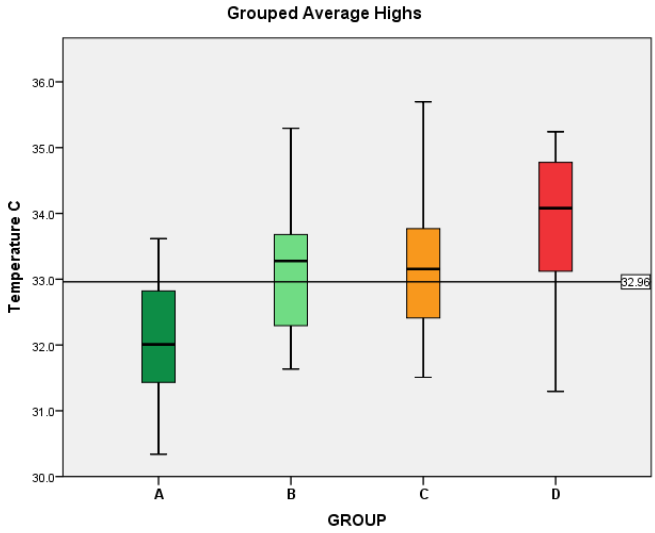

Figure 13. A box plot graph comparing the medians of the average high temperatures separated into their respective groups. The solid line represents the median temperature from the sensors. The dark lines inside the colored boxes lie at the medians for those groups.

The median value for Group A was 32.0° C (89.6° F) and that group also displayed the least amount of difference between the coldest and hottest averaged high temperatures (3.27° C). The Group B median was 33.27° C (91.89° F) and had a range of 3.66° C. Group C's median (33.15° C; 91.67° F) was slightly lower than Group B's. That group had the widest range between its extreme values (4.18° C). The Group D median value was 34.08° C (93.34° F) and its range was 3.94° C. Table 2 is a summary of those statistics for the grouped average high temperatures.

Table 2. Descriptive statistics for the grouped average high temperatures.

Group	Mean	Median	St. Dev.	Min	Max	Range	Dep. Avg.
A	32.04	32.00	0.89	30.34	33.61	3.27	-0.95
B	33.11	33.27	1.07	31.63	35.29	3.66	0.12
C	33.22	33.15	1.14	31.51	35.70	4.18	0.23
D	33.80	34.08	1.18	31.29	35.24	3.94	0.80

A Kruskall-Wallis difference of means analysis was performed on the high temperature data. Again, the Kruskall-Wallis test result (p-value < .001) indicated that a significant difference existed between at least one of the groups. For that reason the groups were paired against each other again using the Mann-Whitney U test statistic. The results of these tests indicated that Group A was significantly different from all other groups and the average high temperatures in that group were the lowest (p-values <.003). Groups B and C did not display a statistically significant difference from each other (p-value .73). Group D was significantly different from Groups A and B (p-value .046) but did not differ significantly from Group C (p-value .65). This grouping pattern (A, BC, CD) still shows the trend of average temperatures increasing in order from Group A to Group D. This means that sensors in areas of with more pervious surface cover are cooler than areas with more impervious surface cover. Sensors with more than 25% of impervious surface cover in their vicinities are warmer but average temperatures overlap between those groups more, so they are less statistically distinct in groups B, C, and D.

4.3 Average Low Temperatures

The average of all the daily low temperatures record by the sensors during the study was 17.75° C (63.95° F). The sensor which recorded the lowest averaged daily low temperature was # 16 (Group A). That sensor's daily low average was 16.21° C (61.18° F). The sensor which recorded the highest averaged daily low temperature was # 85 (Group D). The average daily low temperature from sensor #85 was 18.96° C (66.13° F). There was a difference of 2.75° C between the highest and the lowest averaged daily low temperatures.

Figure 14 is an IDW raster generated using the averaged daily low temperatures. The same thermal pattern showing warmer areas along the western and eastern edges of campus remains when mapping the averaged low temperature data. As expected, the cooler regions are in places mostly covered by turf grass and vegetation. This is a pattern similar to a study in Phoenix, Arizona, which showed a consistent pattern of warmer low temperatures associated with downtown regions (similar to Group D) there (Balling 1987).

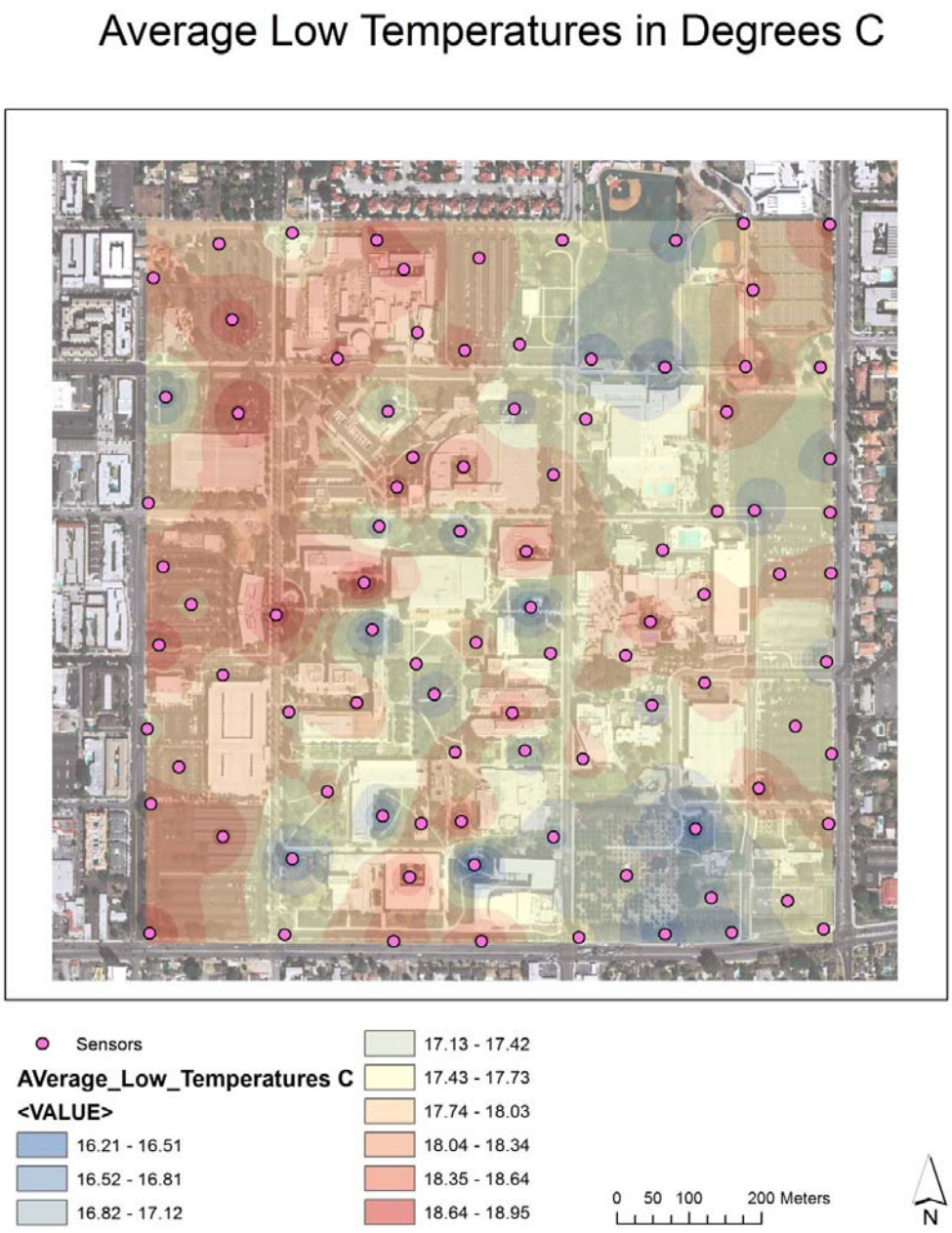

Figure 14. An IDW raster created by using the averages of the daily low temperatures and estimating temperatures in between them based on distance from known values.

The average low temperature data were plotted and examined to determine if there was a relationship between the percentage of impervious surface cover surrounding

sensors and the average low temperatures recorded over the study period. A Pearson product-moment correlation coefficient was computed to assess the strength and direction of that relationship. The results of that test (r^2=.365, r=.60, n= 93, p=.000) indicated that a moderately positive correlation exists between those variables (r=.60). The r^2 value of .365 means approximately 36% of the variation in the average low temperatures can be explained by differences in the percentage of impervious surface cover near the sensors. There were 93 samples used in the calculation (*n)* and the *p* value of less than .001 indicates a high confidence level in this finding. Figure 15 summarizes those results.

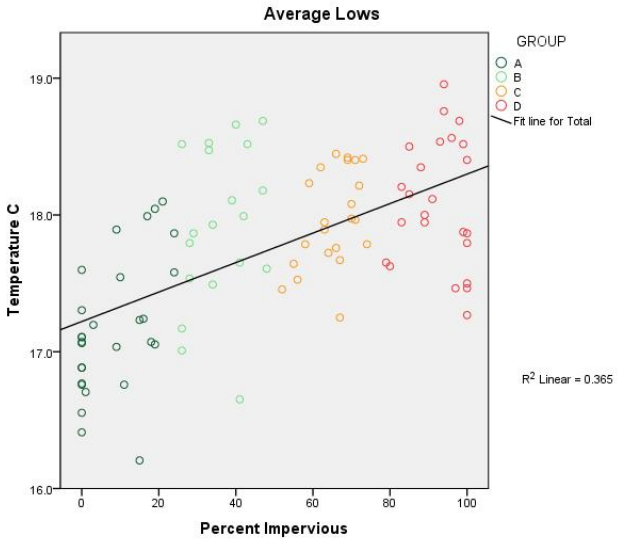

Figure 15. A scatter plot showing the average low temperatures against the percentage of impervious cover surrounding the sensor locations. The Pearson's r correlation coefficient was .60, which is considered a moderately strong positive correlation.

The average of the daily low temperatures from all of the sensors over the two week duration of the study was 17.75° C (63.95° F). The average of the daily low temperatures recorded at CSUN's station was 0.85° C cooler at 16.90° C (62.42° F). Group A had the coolest average daily low temperature, which was 17.18° C (62.92° F).

That group's average was also the most distant from the mean temperature (-0.57° C). Group B's averaged daily low temperature was 17.91° C (64.24° F). This group was the closest to the mean (0.16° C). Group C was warmer (17.97° C; 64.35° F) and exceeded the mean by 0.22° C. The average of Group D's low temperatures was 0.34° C above the mean (18.09° C; 64.56° F). The difference between the hottest and the coldest averaged daily low temperatures was 0.77° C. That data is presented in figure 16.

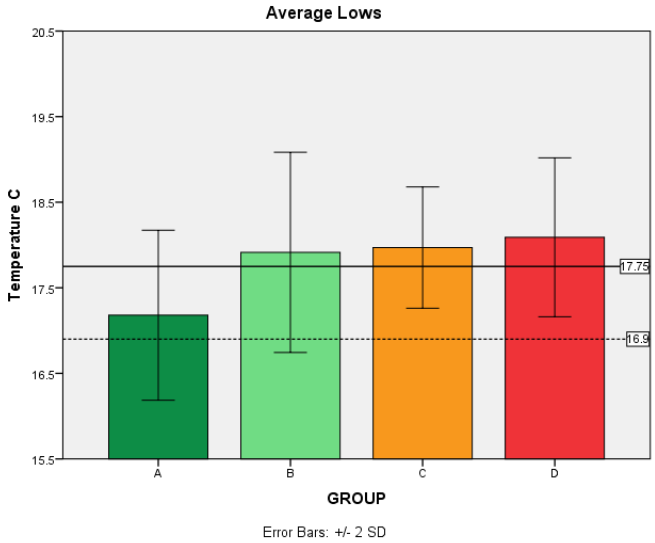

Figure 16. A box plot graph of the grouped average low temperature data along with vertical bars representing two standard deviations from those averages. The solid black line displays the mean temperature from all of the sensors. The dashed line displays the mean temperature recorded at the CSUN weather station during the study period.

Figure 17 displays how the grouped averaged low data were distributed around their medians. The median value was 17.79° C (64.02° F) and that is represented by the horizontal line across the chart. The Group A median is clearly lower than those of the other groups which demonstrated significant statistical overlap in temperature ranges.

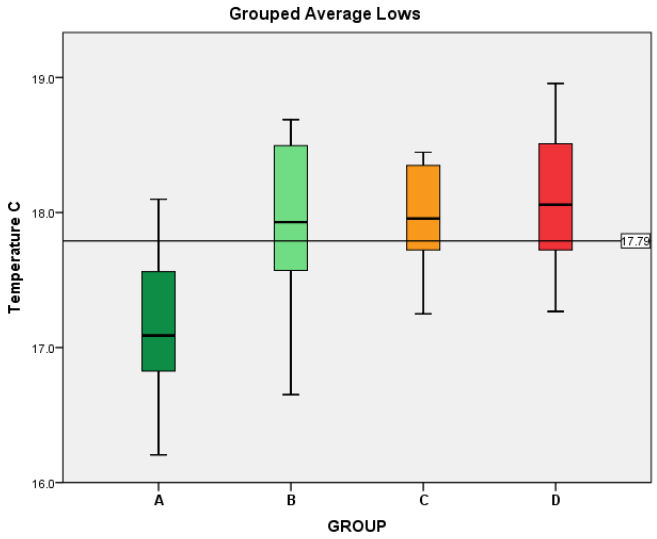

Figure 17. A box plot graph comparing the medians of the average low temperatures separated into their respective groups. The solid line represents the median temperature from the sensors. The dark lines inside the colored boxes lie at the medians for those groups.

The Group A median was 17.09° C (67.76° F) and there was 1.89° C between the hottest and coldest sensor in that group. Group B's median was 17.96° C (64.33° F) and that group had the largest range in values, which was 2.04° C. Group C's median was also 17.96° C (64.33° F) but that group's range in values was the lowest (1.2° C). Group D had the highest median (18.09° C; 64.56° F) and its range was 1.69° C. Those results are summarized in Table 3.

Table 3. Descriptive statistics of the grouped average low temperatures data.

Group	Mean	Median	St. Dev.	Min	Max	Range	Dep. Avg.
A	17.18	17.09	0.50	16.21	18.10	1.89	-0.57
B	17.91	17.96	0.58	16.65	18.69	2.04	0.16
C	17.97	17.96	0.35	17.25	18.45	1.20	0.22
D	18.09	18.06	0.46	17.27	18.96	1.69	0.34

The Kruskall-Wallis difference of means tests resulted in a *p*-value of less than .001, so there was at least one group which was statistically different from the others. The Mann Whitney tests were conducted to determine which groups were statistically distinct. The results of these tests indicated that Group A was statistically distinct from all the others while Groups B, C and D were not statistically distinct.

4.4 Temporal Analysis

4.4.1 Averaged Hourly Temperatures

The grouped mean temperatures for each hour were computed and graphed in figure 18. The warmest hour was 4:00 PM among all groups. That hour's average temperature was 32.41° C (90.34° F). The sensor with the warmest average at that hour was # 53 (Group C). Its temperature of 35.21° C (95.37° F) exceeded the mean for that

hour by 2.8° C. Sensor # 53 was located between the University Student Union building and the newly built sports complex, close to the middle and eastern portion of campus. The lowest average temperature was at 6:00 AM in all groups and that was 17.97° C (64.35° F). The sensor with the lowest average at that time was # 16 (Group A). Sensor # 16, located at the northwest corner of the Performing Arts Center, averaged 16.37° C, which was 1.6° C below the mean temperature at that time. Figure 18 is a graph of the averaged hourly temperature data by group.

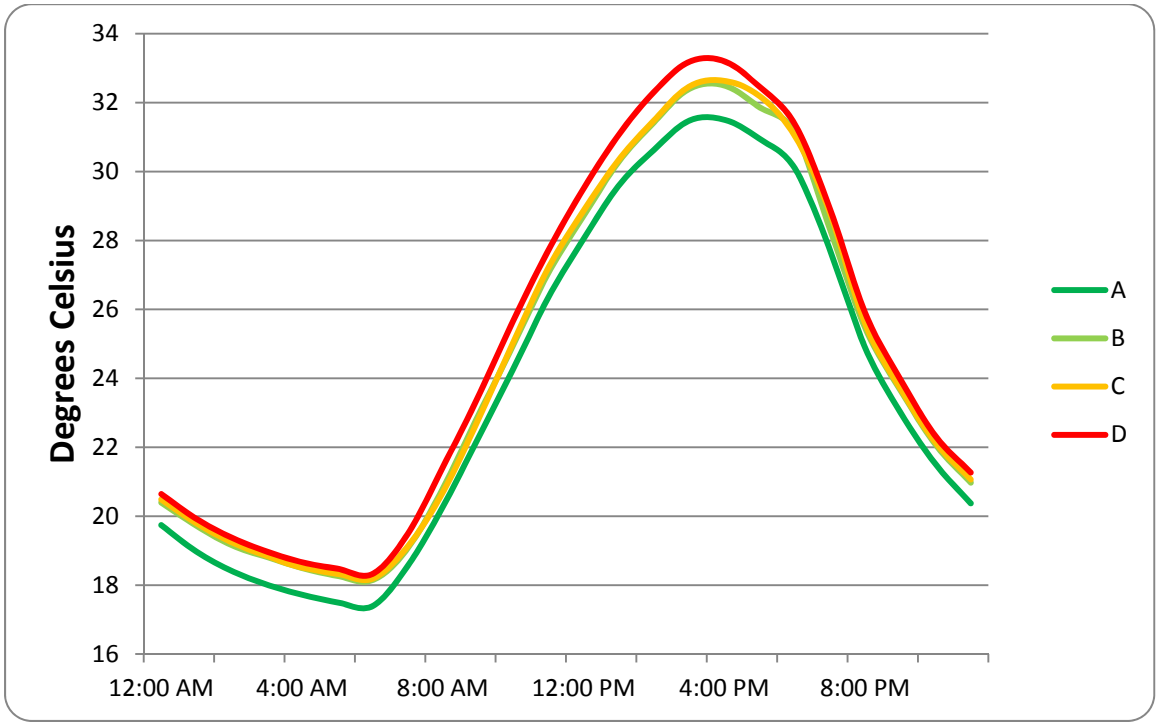

Figure 18. The average hourly temperatures during the study by group. The warmest hour on average was 4 PM. The coolest average hour was 6 AM.

These averaged hourly temperatures separated by group show that Group A remained cooler than the other groups at all hours. This pattern differs from some UHI studies which found urban centers (similar in nature to Group D) could be slightly cooler than their surroundings during the first few hours following sunrise. Fabrizi (2010) and Sullivan (2009) both noted an "urban cool island" effect in their studies which they attributed to thermal capacity and inertia variations between cities and their surroundings. Specifically, they found that urban areas continued to cool even as parts of them were beginning to warm from a newly rising sun. This caused a lag time in urban heating until around noon when the UHI pattern reemerged.

4.4.2 Analysis of Variance, Grouped Hourly Averages

Kruskall-Wallis statistical tests with a 95% confidence level were applied to each hour's grouped data. The results of these tests indicated that there were statistically significant differences among the groups for every hour. That test did not demonstrate which groups differed from each other; however, Mann-Whitney tests were then applied to the grouped data sets to check for statistically significant differences amongst groups. The results of these tests are displayed in table 4. Those paired tests indicated that there were only three statistically distinct groups at most for any hour, and for the hours between 11:00 PM and 7:00 AM only two distinct groupings existed. Group A was distinct and cooler at all hours except for 8:00 AM when some overlap with Group C occurred. Groups B and C were consistently indistinguishable at all hours. Group D was distinct from the other groups at some hours but at times was indistinguishable from Group C. Group D also overlapped significantly with Group B at the 9:00 AM hour.

Table 4. Statistical analysis of variance tests.

Hour	Stat Group 1	Stat Group 2	Stat Group 3
12 – 7 AM	A	BCD	
8 AM	AC	BC	D
9 AM	A	BC	BD
10 AM	A	BC	D
11 AM	A	BCD	
12 PM	A	BC	D
1 PM	A	BC	D
2 PM	A	BC	D
3 PM	A	BC	D
4 PM	A	BC	CD
5 PM	A	BC	CD
6 PM	A	BCD	
7 PM	A	BCD	
8 PM	A	BC	D
9 PM	A	BC	D
10 PM	A	BC	CD
11 PM	A	BCD	

These analyses of grouped hourly temperature averages demonstrate, in part, some of the thermal inertia dynamics presented by Fabrizi (2010) and Sullivan (2009). While Group D never dropped below the other groups in average temperature, there was much more mixing of statistical groupings between the hours of 8:00 and 11:00 AM. These are roughly the same hours in which those studies reported cooler areas in urban centers than their rural surroundings. That process may be responsible for the wide variety of statistical overlap between the groups in those morning hours in this study.

The statistical group pairings for the 6:00 and 7:00 PM hours still show Group A as statistically distinct, but the other groups lose statistical distinction at those hours. It is unclear what the reason behind that variation may be. One possibility is that winds increase later in the day. The average wind speed at those hours was 3.7 miles per hour at the weather station on campus. This follows a peak in winds at 3:00 PM (averaging 4.3 mph). That windiness, combined with less solar radiation heating the ground in those hours may account for the lack of statistical distinctions between groups B, C and D at those hours. Still, the most noticeable feature of those groupings is Group A's consistent distinction from the other groups at all hours except 8:00 AM.

4.5 Warmest Average Hour

The hour with the highest average temperature was 4:00 PM. That average was 32.41° C (90.34° F). The sensor which recorded the lowest average temperature at that hour was sensor # 97 (Group A); that average was 30.06° C (86.11° F). The sensor with the highest average temperature at that time was # 53 (Group C); its average 4:00 PM temperature was 35.21° C (95.38° F). There was a difference of 5.15° C between the highest and the lowest average 4:00 PM temperatures.

Figure 19 is an inverse distance weighted raster created using the average 4:00 PM temperature data. Again, the general pattern shows the highest temperatures are associated with parking lots and more built up areas on campus. The cooler areas are found more in the central regions which contain larger areas of irrigated landscaping. The 5.15° C range between the hottest and coldest locations are very consistent with a heat island study in Westfield, Massachusetts which demonstrates a difference of 6° C between that city and its surroundings (Bristow 2010).

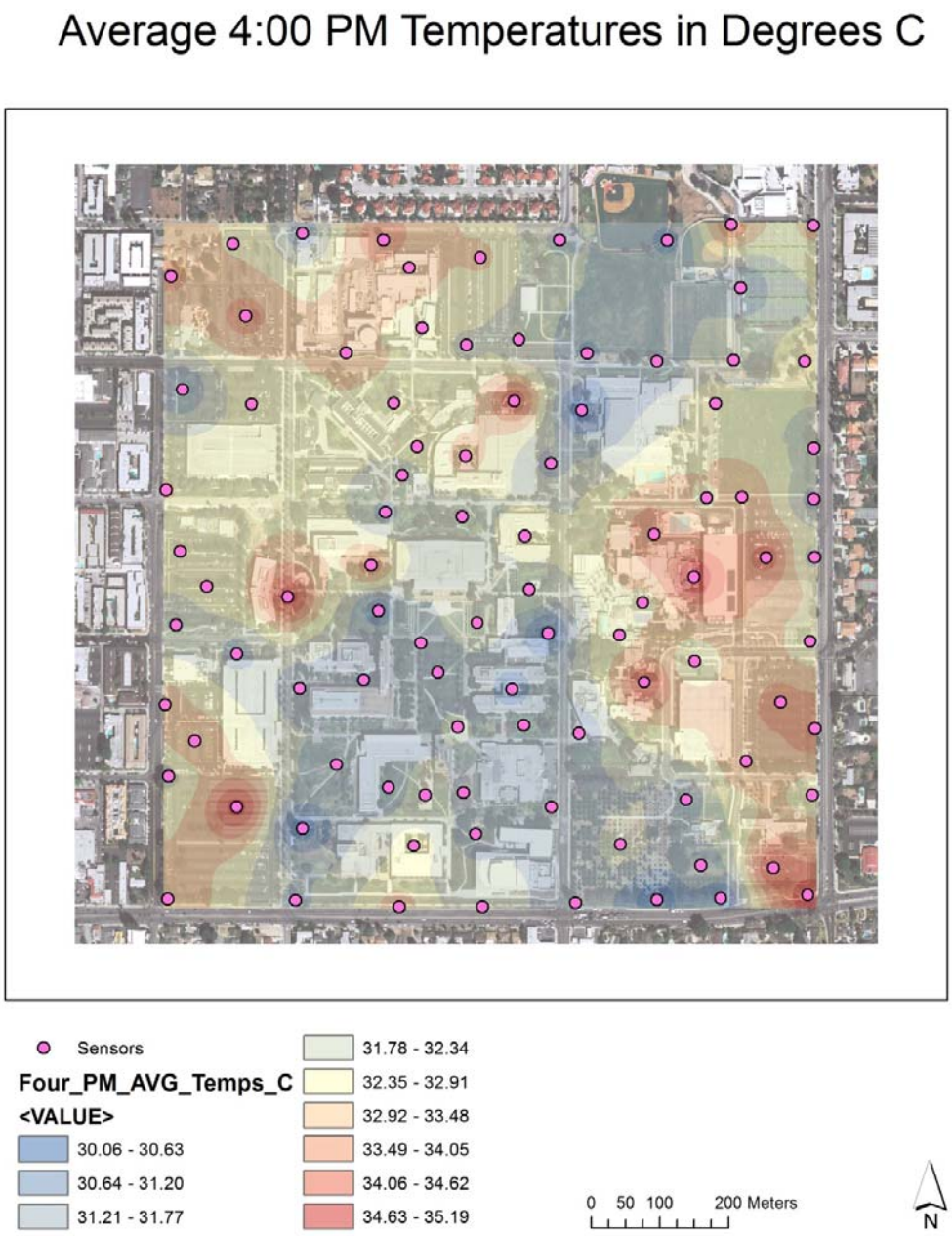

Figure 19. An IDW raster created by using the average 4 PM temperatures and estimating temperatures in between them based on distance from known values.

.

4.5.1 Correlation Analysis, Warmest Average Hour

The average of the temperature data from the 4:00 PM hour were plotted and examined to determine if there was a relationship between the percentage of impervious surface cover surrounding sensors and the average 4:00 PM temperatures recorded A Pearson product-moment correlation coefficient was computed to assess the strength and direction of that relationship. The results of that test (r^2=.344, r=0.58, n= 93, p=.000) indicated that a moderately positive correlation exists between those variables (r=0.58). The r^2 value means that about 34% of the variation in average 4:00 PM temperatures can be explained by differences in the amount of impervious surface cover near the sensors. There were 93 samples used in the calculation (*n)* and the *p* value of less than .001 indicates a high confidence level in this finding. Figure 20 summarizes those results.

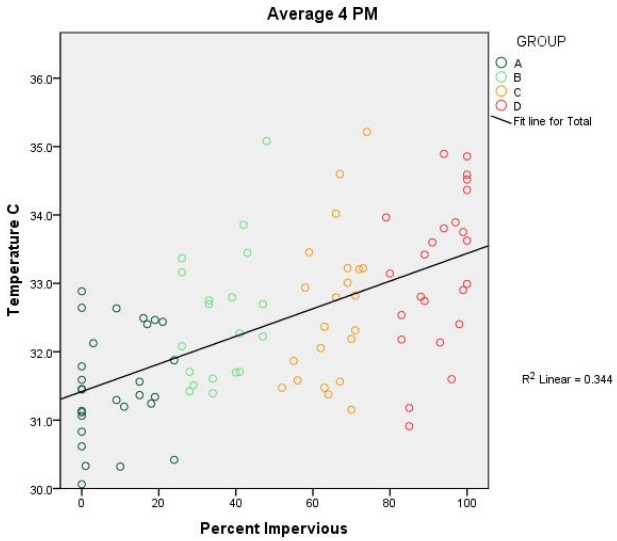

Figure 20. A scatter plot showing the average 4 PM temperatures against the percentage of impervious surface cover surrounding the sensor locations. The Pearson's r correlation coefficient was .58, which is considered a moderately strong positive correlation.

4.5.2 Grouped Analysis, Warmest Average Hour

The average of the 4:00 PM temperatures was 32.41° C (90.34° F). Group A had the lowest average temperature (31.5° C; 88.7° F) as well as the greatest variation from the mean (-0.91° C). Group B averaged slightly higher at 32.5° C (90.5° F) and was only 0.09° C above the mean. Group C was warmer still with an average of 32.63° C (90.73° F) which was 0.22° C higher than the mean. Group D was the warmest (33.2° C; 91.76° F) and exceeded the mean by 0.79° C. The CSUN weather station's 4:00 PM average temperature was 31.66° C (90.79° F). Those comparisons are displayed in figure 21.

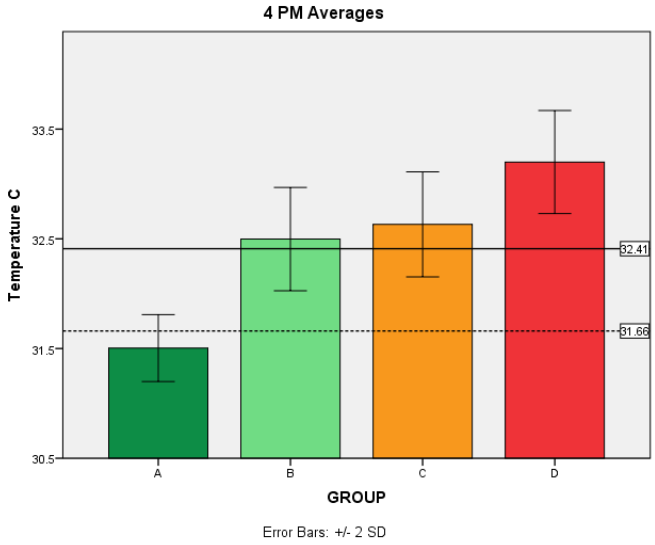

Figure 21. The grouped average 4 PM temperature data along with vertical bars representing two standard deviations from those averages. The solid black line displays the mean temperature from all of the sensors. The dashed line displays the mean temperature recorded at the CSUN weather station during the study period.

Figure 22 displays the median value 4:00 PM daily averages as well as the distribution of those values once grouped. The median of all the 4:00 PM averaged temperatures was 32.37° C (90.27° F). This chart shows that most of the temperatures in Group A fell below the overall median. The medians from Group B and Group C were close, while Group C and Group D displayed a great deal of overlap in the range of the average 4:00 PM temperatures.

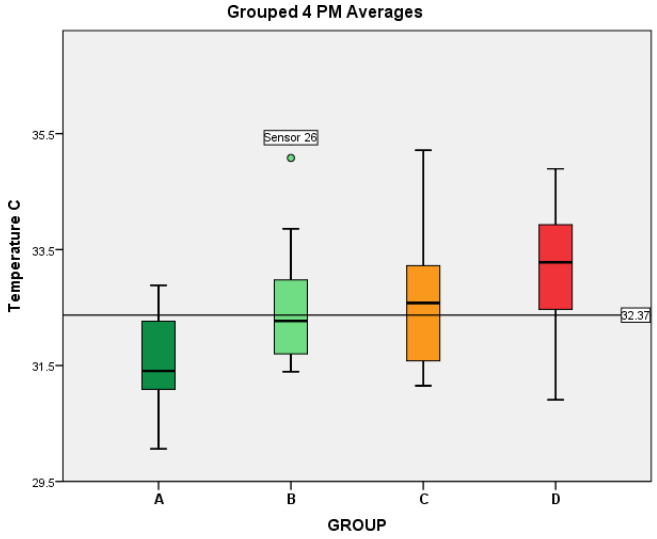

Figure 22. A box plot graph comparing the medians of the 4 PM average temperatures separated into their respective groups. The solid line represents the median temperature from the sensors. The dark lines inside the colored boxes lie at the medians for those groups.

Group A had the lowest median (31.41° C; 88.54° C) as well as the smallest range between coldest and hottest values (2.82° C). Group B's median was 32.27° C (90.09° F) and had a range of 3.69° C. There was an outlier in Group B at sensor #26 which was located at the extreme south and eastern end of campus near a parking lot and large thoroughfare (Nordhoff Ave.). That outlying value (35.08° C; 95.14° F) was 1.22° C

higher than the next warmest sensor in that group (possible reasons for that outlier will be discussed later). The Group C median was 32.58° C (90.64° F) and its range was widest (4.06° C). Group D's median was 33.28° C (91.9° F) and its range was 3.98° C. Table 5 shows how the means and medians compared for these grouped data.

Table 5. Descriptive statistics for the grouped 4 PM average data.

Group	Mean	Median	St. Dev.	Min	Max	Range	Dep. Avg.
A	31.50	31.41	0.79	30.06	32.88	2.82	-0.91
B	32.50	32.27	0.98	31.39	35.08	3.69	0.09
C	32.63	32.58	1.08	31.15	35.21	4.06	0.22
D	33.20	33.28	1.11	30.91	34.89	3.98	0.79

The Kruskall-Wallis tests for the grouped average 4:00 PM data displayed three distinct groups. Group A was distinctly different from all of the others and was coldest. When Group A was paired with Group B, the *p*-value was .001, against the other groups, the *p*-values were less than .001, so there is a high confidence level in classifying Group A apart from the other groups. Groups B and C were not statistically different from each other. The *p*-value resulting from that pairing was .685. Group D overlapped enough with Group C (*p*-value of .079) so that those two groups were not statistically different at the 95% confidence level; however, it was significantly different from Group B (*p*-value

.030). This pattern (A, BC, CD) shows again that Group A is consistently distinct from the other groups, and sensors with intermediate and high percentages of impervious surface cover are less statistically distinct from each other.

4.6 Coolest Average Hour

The hour with the lowest average temperatures was 6:00 AM. The average temperature at that hour was 17.97° C (64.35° F). The sensor with the lowest temperature (116.37° C; 61.47° F) was #16, Group A. That was 1.5° C below the mean. The sensor with the warmest temperature (19.24° C; 66.63° F) was # 85, Group D. That was 1.27° C above the mean. There was a difference of 2.88° C between the highest and the lowest 6:00 AM average temperatures.

Figure 23 is an IDW raster created using that data. This map is very similar to the map of averaged low temperatures. The range in temperature difference between this map and the map of average low temperatures is only 0.13° C. These smaller ranges between the hottest and coldest sensors demonstrate how temperatures differences are greatly reduced among all areas during the coolest hours, even as many warmer areas persist. While beyond the scope of this study, this map also suggests that sky view factor and building geometries, by preventing wind flow and interfering with outgoing thermal radiation from the surface, may be preventing some locations from cooling during the overnight hours. Several of the sensors partly enclosed by, or in near proximities to buildings appear warmer than is the case in most of the other maps. The pattern of the coldest temperatures in areas with lawn cover is also evident, as expected.

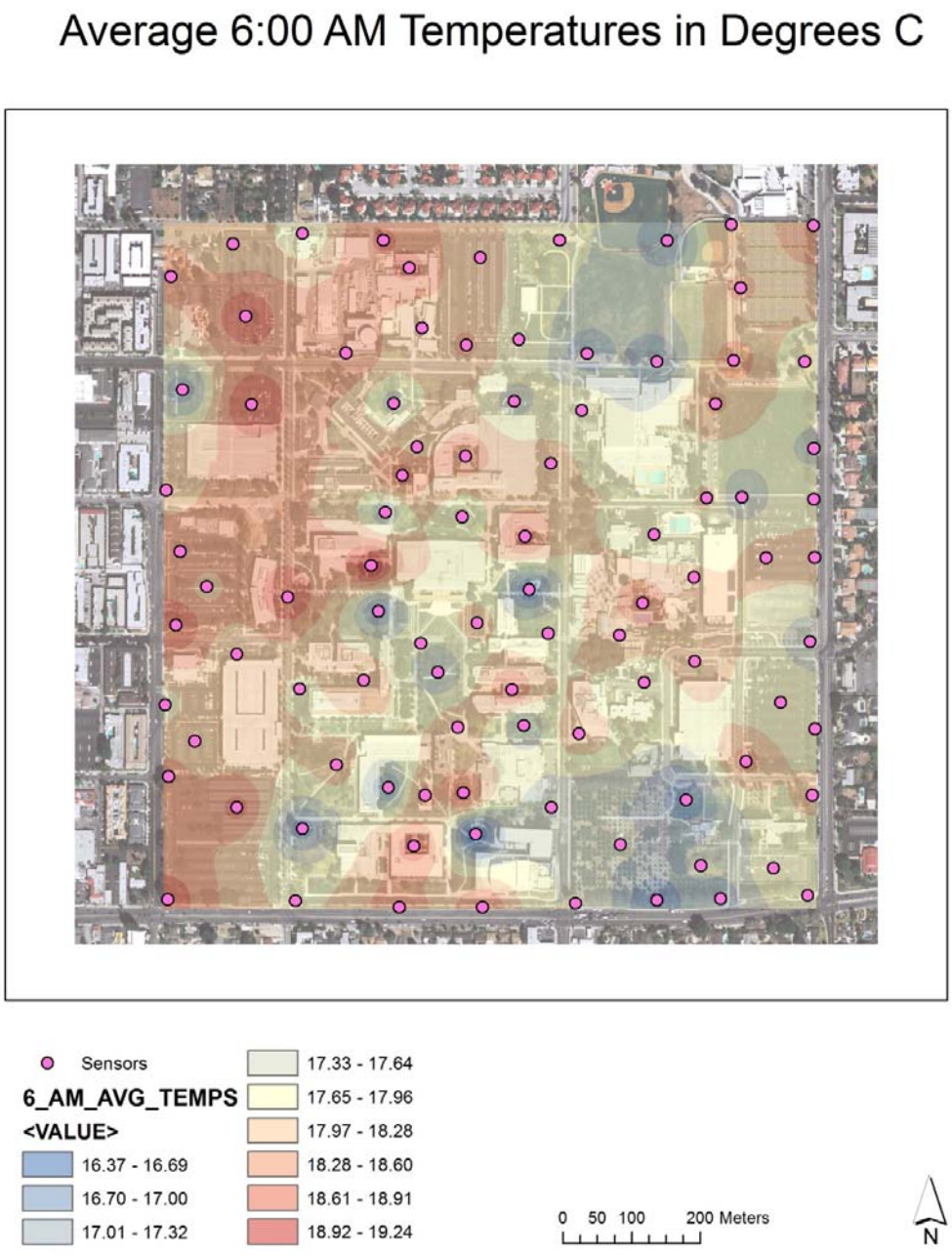

Figure 23. An IDW raster created by using the averages of the 6:00 AM temperatures and estimating temperatures in between them based on distance from known values.

4.6.1 Correlation Analysis, Coolest Average Hour

The average of the temperature data from the 6:00 AM hour was plotted and examined to determine if there was a relationship between the percentage of impervious surface cover surrounding sensors and the average 6:00 AM temperatures recorded. A Pearson product-moment correlation coefficient was computed to assess the strength and direction of that relationship. The results of that test (r^2=.372, r =0.61, n= 93, p=.000) indicated that a moderately positive correlation exists between those variables (r =0.61). The r^2 value means that nearly 37% of the variation in average 6:00 AM temperatures can be explained by differences in the amount of impervious surface cover near the sensors. There were 93 samples used in the calculation (*n)* and the *p* value of less than .001 indicates a high confidence level in this finding. Figure 24 displays those results.

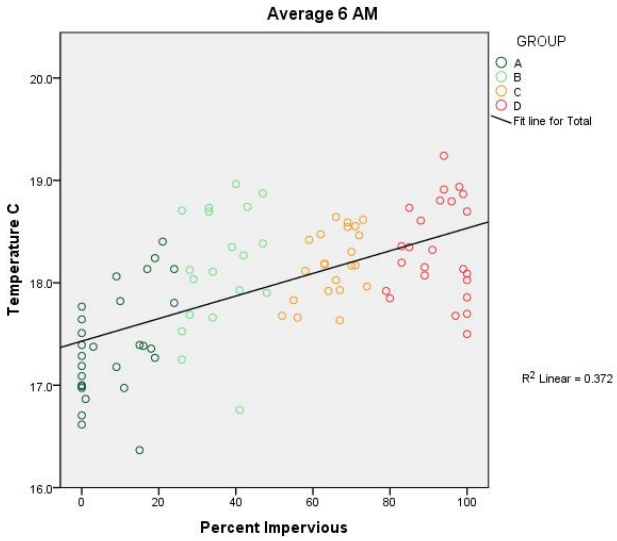

Figure 24. A scatter plot showing the average 6 AM temperatures against the percentage of impervious surface cover surrounding the sensor locations. The Pearson's r correlation coefficient was .61, which is considered a moderately strong positive correlation.

4.6.2 Grouped Coolest Average Hour

The average temperature at 6:00 AM was 17.97° C (64.34° F). The Group A average was 17.39° C (63.3° F). That group was the coolest with the most variation from the mean (-0.58° C). The Group B average of 18.14° C (64.65° F) was nearest to the mean, exceeding it by only 0.17° C. Group C averaged 18.19° C (64.74° F) and exceeded the mean by 0.22° C. Group D had the warmest average at 18.32° C (64.98° F) and exceeded the mean by 0.35° C. The corresponding CSUN temperature at that time was 17.16° C (62.89° F). Those data are graphed in figure 25.

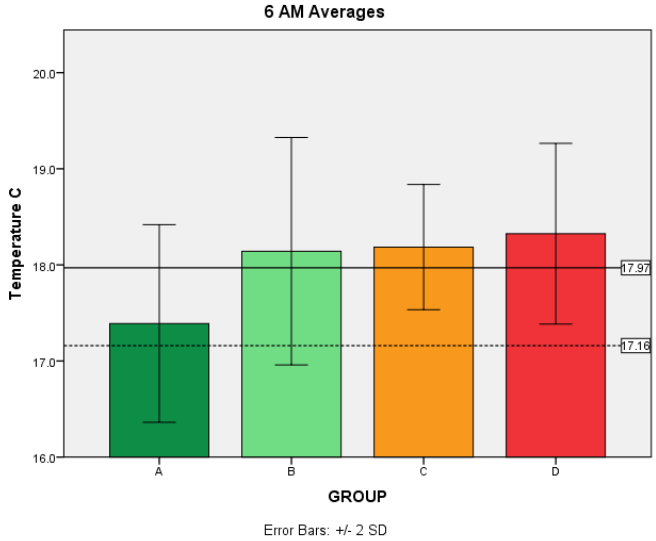

Figure 25. The grouped average 6 AM temperature data along with vertical bars representing two standard deviations from those averages. The solid black line displays the mean temperature from all of the sensors. The dashed line displays the mean temperature recorded at the CSUN weather station during the study period.

.

The median value of the average 6:00 AM temperatures was 18.06° C (64.51° F). Figure 26 is a box plot chart displaying that median as well as the distributions of the grouped data around their respective medians. In that chart, it is evident that Group A contains lower temperatures than the other groups. It also displays that a great deal of overlap in temperature ranges among groups occurs, especially in groups B, C and D.

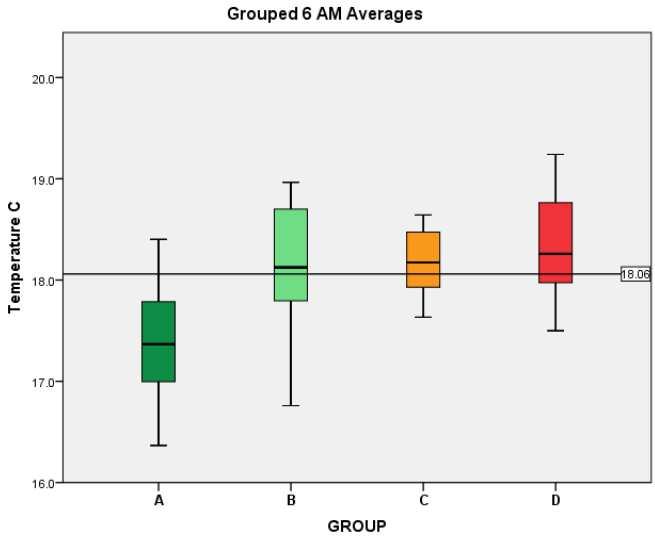

Figure 26. A box plot graph comparing the medians of the average 6 AM temperatures separated into their respective groups. The solid line represents the median temperature from the sensors. The dark lines inside the colored boxes lie at the medians for those groups.

Group A's median was 17.37° C (63.27° F). The range of values between its highest and lowest temperatures was 2.03° C. Group B's median was 18.13° C (64.63° F) and its range was the greatest among groups (2.20° C). Group C's median was 18.17° C (64.71° F) and its range of values spanned 1.01° C. The Group D median value was the highest at 18.26° C (64.87° F) and its range was 1.74° C. A comparison of those means and medians, along with other statistics, are listed in Table 6.

Table 6. Descriptive statistics of the grouped 6 AM average data.

Group	Mean	Median	St. Dev.	Min	Max	Range	Dep. Avg.
A	17.39	17.37	0.51	16.37	18.40	2.03	-0.58
B	18.14	18.13	0.59	16.76	18.96	2.20	0.17
C	18.19	18.17	0.33	17.63	18.64	1.01	0.22
D	18.32	18.26	0.47	17.50	19.24	1.74	0.35

Application of the Kruskall-Wallis statistical test indicated that there was a significant difference among at least one of the groups, so the Mann-Whitney paired tests were conducted on the grouped average 6:00 AM data. For that hour, the only identified statistically different group was Group A ($p<.001$). The differences between Groups B, C and D were negligible at that hour. This grouping pattern (A, BCD) is consistent with the average low temperature pattern and the hourly grouping patterns between midnight and 7:00 AM. The sensors with the highest percentages of pervious surface cover in their vicinities are significantly cooler than those with moderate to high percentages of impervious surface cover.

4.7 Hour of Maximum Temperatures

The warmest hour during the study was at 4:00 PM on July 10, 2012. The mean at that time was 39.24° C (102.6° F); (CSUN weather station was 38.44° C; 101.19° F). The lowest temperature at that hour was 35.63° C (96.13° F). That was at sensor # 50 (Group A). The highest temperature was 43.6° C (110.3° F). That temperature was recorded at two locations. One was sensor # 53 (Group C) and the other was at # 49 (Group D). The difference between the lowest and the highest temperatures at that time was 7.88° C (14.17° F).

Figure 27 is an IDW raster created using that data. While the same general pattern exists in this map, this map also demonstrates the greatest difference between the hottest and coldest sensors. That 7.88° C (14.17° F) difference in air temperatures is less than the differences in surface temperatures recorded at the same time. Surfaces measured with an infrared thermometer on roads and parking lots at that hour were as high as 62.77° C (145° F). Grass and other vegetation surface temperatures were as low as 35° C (96° F). The difference between actual surfaces measure at that hour was 27.22° C (49° F). While those differences are considerable, other studies have shown surface temperature differences as high as 50° C (90° F) at times (Unitted States Environmental Protection Agency 2014). These surface temperatures vary greatly over short distances and that complexity presents challenges when assessing UHI patterns in many instances.

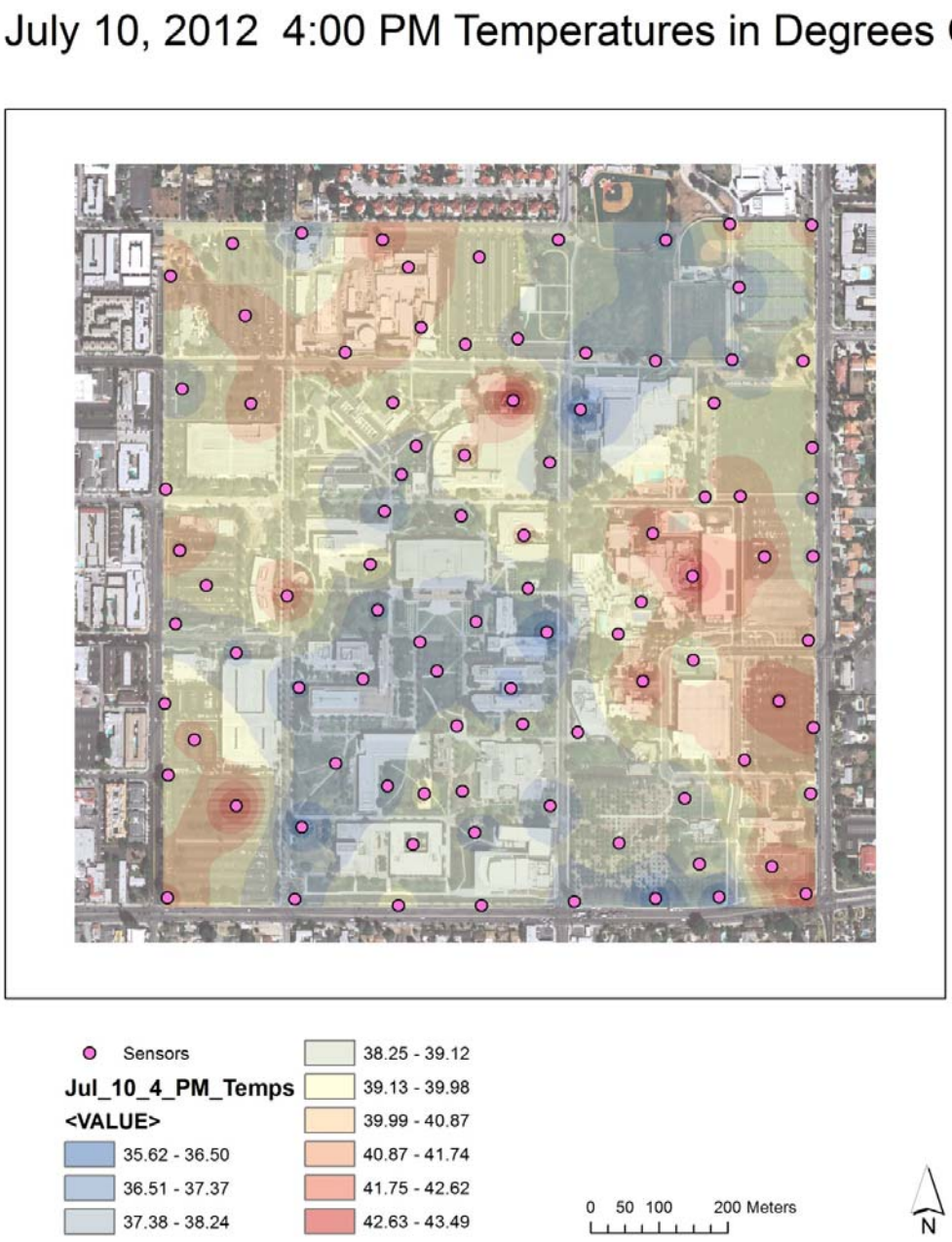

Figure 27. An IDW raster created by using the data from July 10, 2012 at 4 PM and estimating temperatures in between them based on distance from known values.

Because surface temperatures may be considerably hotter than the air temperatures above them, temperatures are commonly measured at 1.5 meters above the

ground. Air is a poor conductor of temperatures, so temperatures usually decline sharply in the first meter above the ground before leveling off (Lyndon State College Atmospheric Sciences 2005). That process is demonstrated in Figure 28. Even though temperatures are recorded at heights 1.5 meters above ground level, the effects of underlying surfaces affect local areas and microclimates significantly.

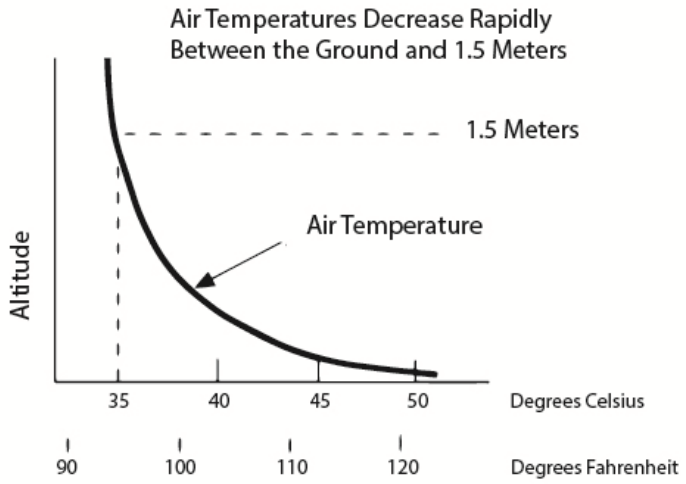

Figure 28. A generalized display of how temperatures decrease rapidly as the distance from the ground increases to near 1.5 meters above it.

4.7.1 Correlation Analysis of Warmest Hour

The temperature data from warmest hour were plotted and examined to determine if there was a relationship between the percentage of impervious surface cover near sensors and the air temperatures recorded at that time. A Pearson product-moment correlation coefficient was computed to assess the strength and direction of that relationship. The results of that test (r^2=.301, r=0.54, n= 93, p=.000) indicated a

moderately positive correlation between those variables (r=0.54). The r^2 value means that roughly 30% of the variation in July 10, 2012's 4:00 PM temperatures can be explained by changes in the percentage of impervious surface cover near the sensors. There were 93 samples used in the calculation (*n)* and the *p* value of less than .001 indicates a high confidence level in this finding. Figure 29 summarizes those results.

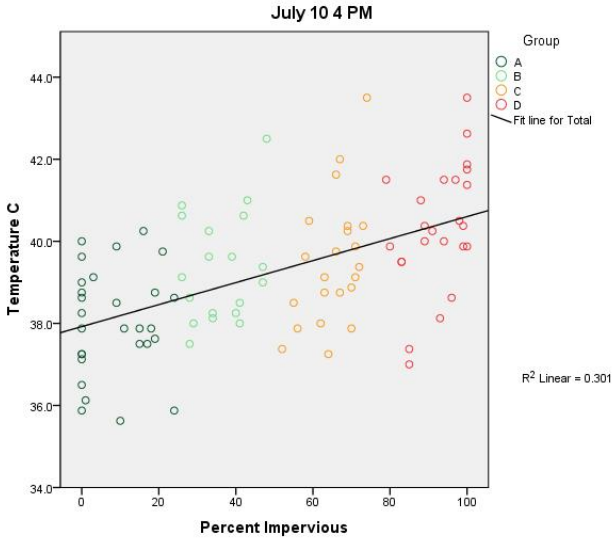

Figure 29. A scatter plot showing the air temperatures recorded at 4 PM on the warmest day of the study against the percentage of impervious surface cover surrounding the sensor locations. The Pearson's r correlation coefficient was .54, which is considered a moderately strong positive correlation.

4.7.2 Grouped Analysis, Warmest Hour

The average temperature at 4:00 PM on July 10, 2012 was 39.24° C (102.63° F). The CSUN station's average at that time was 0.8° C cooler (38.44° C; 101.19° F). The Group A average was 38.03° C (100.45° F). That group was the coldest as well as the most distant from the mean temperature (-1.21° C). Group B's average was 39.36° C (102.85° F). That group was closest to the mean, exceeding it by only 0.12° C. Group C

averaged 39.49° C (103.08° F) and exceeded the mean by 0.25° C. Group D had the warmest average (40.33° C; 104.6° F) and that was 1.09° C above the mean. Figure 30 displays those grouped averages at that hour.

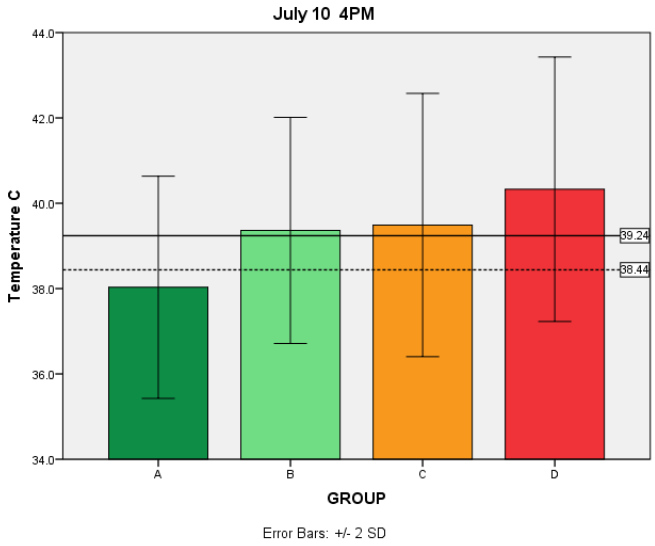

Figure 30. The grouped temperature data from 4 PM on the warmest day along with vertical bars representing two standard deviations from those averages. The solid black line displays the mean temperature from all of the sensors. The dashed line displays the mean temperature recorded at the CSUN weather station during the study period.

Group A had the lowest median value at 4:00 PM on July 10, 2012 (37.88° C; 100.18° F). The 4.63° C difference between its coldest and hottest temperatures was also the lowest range among all the groups. Group B's median was 39.13° C (102.43° F) and that group had a range of 5.0° C between its extremes. Group C had a median of 39.25° C (102.65° F) with a range of 6.25° C. This group had an outlier value which occurred at sensor # 53 (that outlier will be discussed later). Group D's median was the highest (40.31° C; 104.56° F). That group also displayed that largest range between its coldest and hottest values, which was 6.5° C. How those groups compare is displayed in figure 31. Table 7 displays statistical information for the grouped data at the warmest hour.

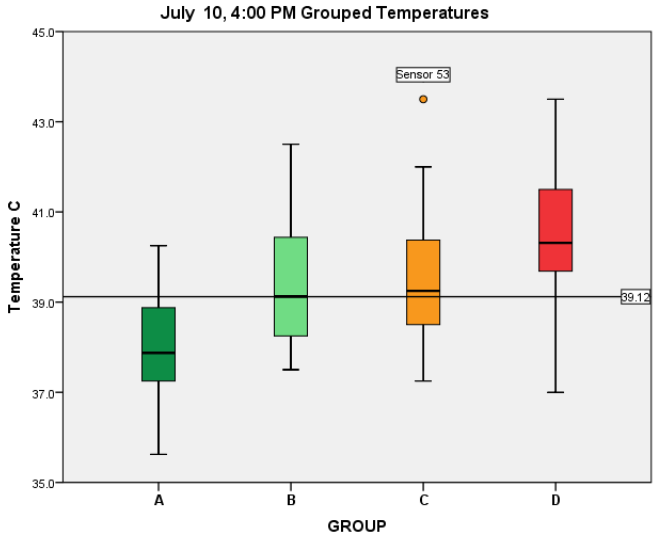

Figure 31. A box plot graph comparing the temperatures at 4 PM on the warmest day separated into their respective groups. The solid line represents the median temperature from the sensors. The dark lines inside the colored boxes lie at the medians for those groups. Group C had an outlier for its class value and that will be examined further in the study.

Table 7. Descriptive statistics of the grouped temperature data from the warmest hour.

Group	Mean	Median	St. Dev.	Min	Max	Range	Dep. Avg.
A	38.03	37.88	1.30	35.63	40.25	4.63	-1.21
B	39.36	39.13	1.32	37.50	42.50	5.00	0.12
C	39.49	39.25	1.54	37.25	43.50	6.25	0.25
D	40.33	40.31	1.55	37.00	43.50	6.50	1.09

The Kruskall-Wallis test indicated that at least one group differed significantly from the others. Mann-Whitney tests were then conducted on the 4:00 PM, July 10, 2013

data. The results of these tests showed two distinct groups. Group A was statistically different from the others with *p*-values only as high as .003. The other groups did not display enough difference to distinguish themselves from each other at that time, so the other group consisted of groups B, C, and D. This statistical grouping pattern (A, BCD) differs from the average high temperature and hottest average hour pattern (A, BC, CD). The consistency of Group A as statistically cooler remains, even as the distinctions between the other groups were not evident at this hour. It is possible that increases in windiness during the afternoon hours may have mixed the air enough to lessen the UHI effects with the exception of the cooling evident in Group A. The average wind speed at that hour was 2.84 mph with a maximum gust of 7.98 mph recorded by the weather station.

4.8 Post Sunset Cooling on Warmest Day

Because UHI effects are most clearly distinguishable after sundown, the hours after sunset on July 10, 2012 were analyzed to determine if any of those effects could be detected. On that date, sunset was at 8:09 PM. The temperatures from 8:00 to 11:00 PM were graphed by their respective group averages. That graph, shown in figure 32 demonstrates how Group A remained the coolest and apart from the other averaged group temperatures as the evening progressed. Group D was initially higher than groups B and C at 8:00 PM. The differences in average temperatures for groups B and C were very close at all hours. Between the hours of 9:00 PM and 11:00 PM, the differences between groups B, C, and D became noticeably closer, and were not statistically distinct after 9:00 PM. This is consistent with the findings in which the cooling effects associated with

surfaces in Group A were stronger than the warming effects of the groups with more impervious surfaces.

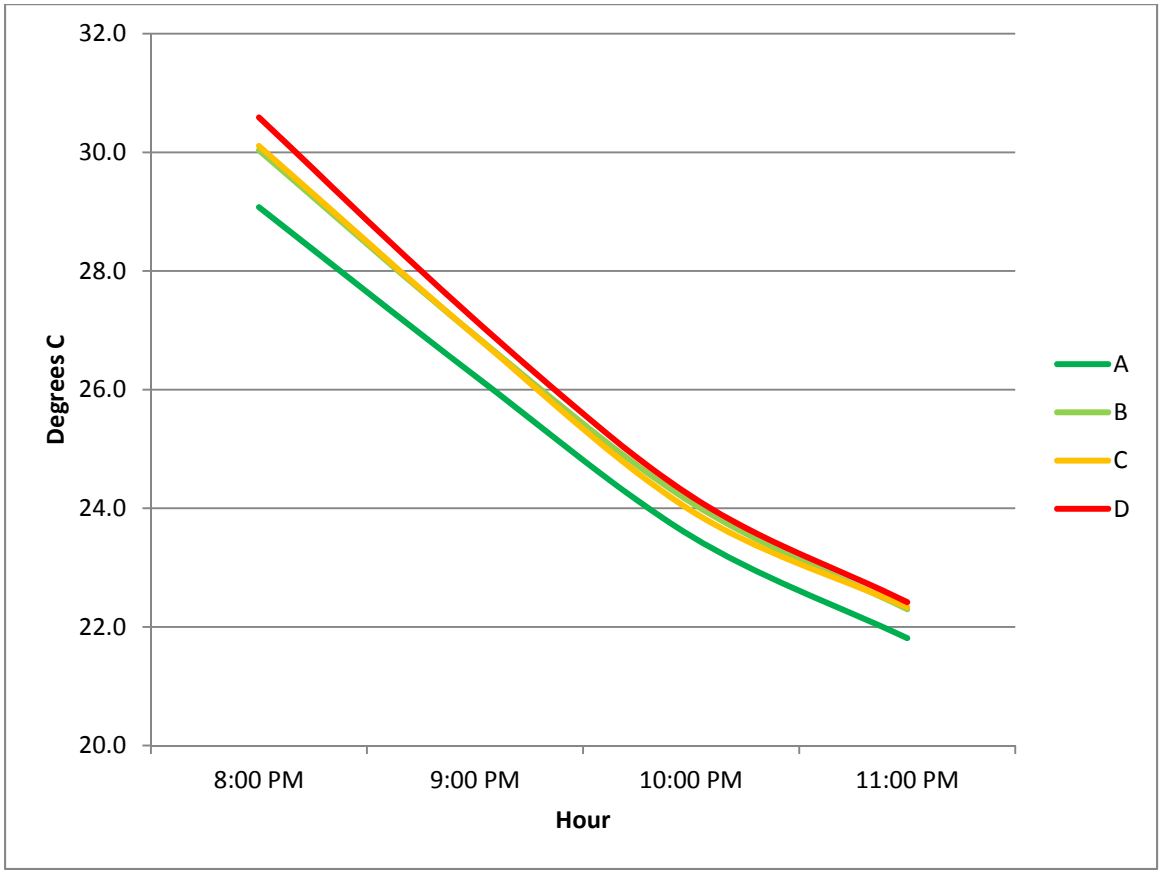

Figure 32. The grouped hourly temperatures from 8 to 11 PM on the warmest day of the study.

4.8.1 Correlation Analysis, Post Sunset on Warmest Day

Pearson product-moment correlation coefficients were computed to assess the strength and direction of the relationships between the percentage of impervious surface cover near sensors and air temperatures between the hours of 8:00 and 11:00 PM on July

10, 2012. The results of these tests indicated that a moderately positive correlation exists between those variables for each of those hours. The highest correlation coefficient (r=0.64) occurred at the 8:00 PM hour. With each passing hour, the correlation coefficients decreased. This means as the evening progressed on the warmest day, the immediate hour after sundown was the most significantly correlated with increased percentages of impervious surface cover near sensor locations. With each passing hour, the correlation was weaker, but still moderately positive. Those hourly correlation coefficients are displayed in table 8.

Table 8. Correlation coefficients data for the evening hours on the warmest day of the study.

Hour	*r*	*n*	*p*
8 PM	.64	93	0.000
9 PM	.59	93	0.000
10 PM	.52	93	0.000
11 PM	.51	93	0.000

4.8.2 Grouped Analysis, Post Sunset on Warmest Day

When the hourly data from the warmest day were statistically analyzed by difference of means tests between 8:00 and 11:00 PM, three distinct groups were identified by the Mann-Whitney tests initially, but only two groups persisted after 9:00

PM. At 8:00 PM, Group A was distinct from all other groups. It remained distinct into the evening. An intermediate group existed at 8:00 PM comprised of groups B and C. Group D was distinct from all other groups at 8:00 PM, but in the following hour that distinction no longer existed. Only Group A remained statistically distinct after 9:00 PM on that day. These findings confirm those from figure 32. Table 9 displays the hourly grouping pattern for those hours.

Table 9. The statistical groupings by hour between 8:00 PM and 11:00 PM on July 12, 2012.

Hour	Stat Group 1	Stat Group 2	Stat Group 3
8:00 PM	A	BC	D
9:00 PM	A	BCD	
10:00 PM	A	BCD	
11:00 PM	A	BCD	

The 8:00 PM grouping pattern demonstrates again how the extremes of impervious or permeable surface cover are much more readily apparent in UHI studies than areas of highly heterogeneous surface types. It was expected that Group D would remain statistically distinct for a longer period into the evening an UHI was being generated on campus.

5 Discussion

The results of this study show that there are UHI generating features on the CSUN campus. These areas are moderately associated with increased percentages of impervious surface cover. While the average temperatures for the warmest areas were higher at all hours, the evening and overnight differences did not remain statistically significant from areas with intermediate amounts of impervious surface cover. Areas of minimal impervious surface cover tended to be significantly cooler than most impervious surface coverings at all times, day and night.

This study did not attempt to determine if the CSUN campus created or existed in an UHI. The groupings did replicate some of the features of those types of studies (i.e. Group A could be likened to open areas or parks, while groups B and C to suburban or less densely developed areas, and Group D had some of the characteristics of dense urban development). When the mean temperatures were compared between groups, the 1.18° C difference between Groups A and D is in reasonable agreement with an estimated average of 2° C warmer temperatures in urban areas compared to their surroundings (Taha 1997). The findings of the greatest differences between those two groups comprising the extremes in permeability are not surprising in light of pre-existing UHI studies.

One reason why areas of greater surface permeability were cooler in this study may be due to the fact that most of the non-impervious surfaces on the CSUN campus are landscaped with irrigated vegetation. For example, of the 28 sensors in Group A, only 5 lacked large sections of lawn grasses. In Southern California, lawns require so much

irrigation that more than half of all residential water use is used for exterior landscaping (United States Environmental Protection Agency 2013). This extra water applied to the permeable surfaces along with the shading that often accompanies vegetation has been shown to offer significant cooling effects which may at times extend hundreds of meters beyond their boundaries (Jin 2012). This study does confirm the findings of numerous other studies that showed cooling effects associated with vegetated areas, such as those that were common in Group A (Hamdi R. & Schayes 2007). While adding vegetation is helpful in preventing UHI development, it does conflict with other issues relating to sustainability, such as the need to reduce water use. Shade producing plants, the type that are also well adapted to drought conditions would be an ideal compromise.

The lack of statistically discernible differences between groups B and C at all times is emblematic of the difficulties of some UHI studies when large amounts of heterogeneous surface types are involved. While the urban to rural differences have been studied extensively, the ways in which very mixed surface types and features interact with and affect air temperatures on multiple scales is still not very well documented (Jin 2012) . Part of the reason is that there are so many different combinations of surface features which do not lend themselves well to classifications. For instance, the vegetation mentioned previously has a high association with the permeable surfaces but there were some areas with less heavily irrigated vegetation as well as alternative surfaces like mulch coverings or even bare soil. For areas of high imperviousness the differences between concrete and asphalt are probably most noticeable because their differences in albedo will likely impact the absorption and reemission of energy significantly. Permeable surfaces, like gravel or hard packed surfaces such as

decomposed granite, may suffer from some of the same heat effects as asphalt or concrete because they may not, especially in July in the San Fernando Valley, produce any evaporative cooling effects, like perhaps grass or ground cover that has measureable evapotranspiration.

Despite the fact that the groups were not always statistically distinct from each other, the values of the temperatures were consistent with Group A<B<C<D. In that way it was consistent with a study in Phoenix (Balling 1987) which documented an UHI at all hours. However, that pattern does differ from the results in a study from Nanjing, China (Huang, et al. 2008) in which air temperatures over vegetated surfaces was slightly higher than those over concrete surfaces during some nighttime hours. That study speculated that a tree canopy's reduction in sky view factor may have caused some vegetated areas to retain warmth better than concrete surfaces that were more open to the sky. Another reason which could explain some of that difference is that Nanjing has a hot and humid climate, while Northridge is generally warm with much lower humidity.

5.1 Outliers

When the data were analyzed by the hourly averages, some hours contained values beyond two standard deviations from the means for their groups. The first one occurred at sensor # 26 (Group B) during the average 4:00 PM temperatures analysis (*sd*=2.64). That sensor's average temperature at that time was 1.22° C higher than the next closest value in that group. There are several factors present at that location which may explain some of that variation and demonstrate the effects of other important variables which were not included in this study.

First of all, sensor # 26, placed at the southeastern corner of campus, was surrounded by 48% impervious surfaces. That places it near the top range of its class (Group B was 26-50% impervious) so it is not surprising that the temperature at this point would be near or at the top of all others in its class based solely on surrounding surface permeability. Even so, there are other factors which may explain some of the excess heat which was present at that sensor during the 4:00 PM hour. There was little shade at that location, so the area was heavily exposed to incoming solar energy. That sensor was located adjacent to Nordhoff Avenue which is a very busy thoroughfare, so another potential source of heat is related to traffic and the exhaust which it produces. Finally, the potential for partial failure of the solar shielding is possible because they were made of aluminum foil which is easily bent. That, along with the likely higher foot traffic at that corner may have increased the odds that curious passersby may have inspected the sensor and shield in a manner which reduced the effectiveness of that shield without leaving any visible evidence upon collection.

The other sensor which provided an outlier value was sensor # 53, Group C. At the warmest hour during the study (4:00 PM on July 10th, 2012) sensor # 53 recorded a temperature of 43.5° C (110.3° F). That was 1.5° C warmer than the next highest temperature in Group C, a value which was 2.39 standard deviations above the group mean. That tied with sensor # 49, Group D, for the warmest temperature from all the sensors during the study. Like sensor # 26, this sensor was near the uppermost limits of its class (impervious surface percentage was 74%; Group D began at 75%). This location also demonstrates how other factors besides permeability need to be taken into account in studies like this one.

Sensor 53 was located between the new Student Recreation Center and the University Student Union buildings. This placed it in what is often referred to as an "urban canyon." Urban canyons are defined by the configurations and orientations of buildings. This may affect air flow and circulation, which may play a role in the unusually high temperatures recorded there. In addition, the orientation of the taller structure on the west may allow for reflected and enhanced solar energy to reach the site, which would also likely raise the temperature at that afternoon hour. Finally, while there was some vegetation present, it was not lawn or heavily irrigated, so some of the cooling associated with the most common vegetation types would not be present at this site. These outliers demonstrate how many other factors besides permeability of surfaces have impacts on air temperatures in various locations.

5.2 Limitations

In addition to the limitations which arose upon examining the outlying data points, there were many other factors which must be addressed. The first limitation affected the placement of the sensors. While a grid pattern of regularly spaced sensors spread out evenly across campus would have been ideal, the building locations and layout prevented that. In areas without obstructions, the centermost points within large homogenous areas were the most desirable but the lack of appropriate mounting structures often prevented those sites from being sampled. That resulted in a less than ideal placement of sensors for this study. Another limitation which arose was the duration of the study. Ideally temperatures could be monitored for longer time periods and in different seasons.

Equipment limitations were also sources of their own limitations. The most immediate shortfall regarding the sensors was the solar shielding. Although shields are available from the manufacturer, the costs were prohibitive. As a result, aluminum foil and Styrofoam shields were employed but were not very durable. The need to shield the devices from direct solar exposure, while at the same time remaining small, allowing air flow and being as inconspicuous as possible, resulted in shielding which may have been compromised at times. Shields that had obviously been damaged resulted in the exclusion of those sensors from the study; however, the possibility that minor failures did occur at times cannot be ruled out.

There are also limitations as to which variables this study was able to incorporate. Even though some of the weather variables, such as wind speed and direction, intensity of incoming solar energy and humidity were available from the CSUN weather station, these were not available for the sensor locations so they were not utilized. Shade is another element which was likely very significant in affecting area temperatures but that was also excluded as a variable because of the difficulties in quantifying the amount of shade due to constant shifting as the sun angle changed.

The effect of buildings and their orientations was also not taken into account for this study. Those aspects are very important in urban microclimate studies because there are vertical surfaces which come with their own thermal effects and as Arnfield (2003) noted it is possible that different sides of buildings could cause more variation in local microclimates than differences in adjacent land use types. That level of analyses was not feasible for this study for the scope and aims of this project. In much the same way, the

sky view factor which is often a very significant factor in night time cooling of urban places was also omitted.

Even the variables which were included in the study had limitations of their own. As already mentioned when describing the outliers, simplifying the surfaces into only impervious or permeable did not allow for differences within those classes to be addressed. Not all impervious surfaces have the same thermal properties and dynamics. There are numerous variations among impervious surfaces. Likewise, the permeable surfaces have variations of their own.

5.3 Future Studies

This study attempted to examine the relationships between common surfaces in a suburban setting and air temperatures. There are still many uncertainties in our understandings of some of these very complicated relationships. Future studies could expand on this one in several ways. One way would be to utilize the same data and incorporate more variables into the calculations to see if other patterns became apparent. Another way would be to change the size of the buffered area surrounding the sensors to determine whether the patterns identified remain, or change significantly when more or less surrounding area is included in making classification determinations. Alternative statistical analyses are another way to utilize the existing data to search for patterns which this study overlooked. This new research may provide useful information.

Other studies which addressed some of the inter class variations in albedo for sensors in Group D, or assessing the differences between highly irrigated and lesser irrigated vegetation would be useful too, especially because of the possibility of water

scarcity leading to changes in the nature of the vegetation covering so many parts of the campus.

6 Conclusion

Even though the mechanisms of Urban Heat Islands are well understood, in many areas the complex mixture of surfaces associated with suburban development creates a mix of both warming and cooling effects. Increases in impervious surfaces resulted in warmer air temperatures on the CSUN campus in this study. Those differences were most significant in the hour immediately following sunset but overnight those differences were much less distinct. It is very likely that the cooling effects of irrigated landscaping had a slightly stronger cooling effect than the warming associated with impervious surfaces in this location. The cooling effects of the more permeable surface areas may have been influenced more strongly than the lack of impervious materials due to the significant amounts of irrigation which are applied to those areas. While the CSUN campus does not exactly match the kind of development in the surrounding areas, it does contain enough similarity to provide some insight into how nearby areas are likely to respond to warm weather in the context of UHI development. Surface permeability is only one factor among many which need to be addressed when studying UHI patterns. Additional factors could be included even on a similar scale to this study.

Bibliography

Akbari, H., M. Pomerantz, and H. Taha. "Cool surfaces and shade trees to reduce energy use and imporve air quality in urban areas." *Solar Energy* 70, no. 3 (2001): 295-310.

Arnfield, John A. "Two decades of urban climate research: A review of turbulence, exchanges of energy and water, and the urban heat island." *International Journal of Climatology* 23 (2003): 1-26.

Balazs, Bernadett, Terianne Hall, Matthias Roth, and Leslie K. Norford. "Microclimate in a high-rise residential development in Singapore." Yokohama, Japan, 2009.

Balling, Robert C. and Brazel, Sandra W. "Time and space characteristics of the Phoenix urban heat island." *Arizona-Nevada Academy of Science* (Arizona-Nevada Academy of Science) 21, no. 2 (1987): 75-81.

BBC News. *Disney hall glare 'heats homes'.* February 24, 2004. http://news.bbc.co.uk/2/hi/entertainment/3516051.stm (accessed November 14, 2011).

Bristow, R., Blackie, R., Brown, N. "Parks and the urban heat island: a longitudinal study in Westield, Massachusetts." *Proceedings of the 2010 Northeastern Recreational Research Symposium.* 2010. 224-230.

Bruse, Michael, and Heribert Fleer. "Simulating surface-plant-air interactions inside urban environments with a three dimensional numerical model." *Environmental Modeling & Software* 13 (1998): 373-384.

Changnon, S. A. "The La Porte weather anomaly-fact or fiction." *Bulletin American Meteorological Society* 49 (1968): 4-11.

Dash, P., F.M. Gottsche, F. S. Oleson, and H. Fischer. "Land surface temperature and emissivity estimation from passive sensor data: Theory and practice-current trends." *International Journal of Remote Sensing* 23, no. 13 (2002): 2563-2594.

Dousset, Benedicte, and Francoise Gourmelon. *Remote sensing applications to the analysis of urban microclimates.* IEEE/ISPRS Joint Workshop on Remote Sensing and Data Fusion over Urban Areas, 1986.

Fabrizi, Roberto, Bonafoni, Stefania, and Biondi, Riccardo. "Satellite and Ground-Based Sensors for the Urban Heat Island Analysis in the City of Rome." *Remote Sensing*, no. 2 (2010): 1400-1415.

Fassig, O. L. "The climate and weather of Baltimore." *Maryland Weather Service*, 1907: 276-283.

Gluch, R., D. A. Quattrochi, and J. C. Luvall. "A multi-scale approach to urban thermal analysis." *Remote Sensing of the Environment* 104 (2005): 123-132.

Hamdi R. & Schayes, G. "Sensitivity study of the urban heat island intensity to urban characteristics." *International Journal of Climatology* 28 (August 2007): 973-982.

Hedquist, B. C. & Brazel, A. J. "Urban, residential and rural climate comparisons from mobile transects and fixed stations: Phoenix, Arizona." *Journal of the Arizona-Nevada Academy of Science* 38 (2006): 77-87.

Heldens, W., U. Heiden, T. Esch, and S. Dech. *Potential of hyperspectral data for urban micro climate analysis.* Frascati, Italy: Proceedings Hyperspectral 2010 Workshop , 2010.

Howard, L. *The Climate of London Vols. I-III.* London, 1833.

Huang, L., J. Li, D. Zhao, and J. Zhu. "A fieldwork study on the diurnal changes of urban microclimate in four types of ground cover and urban heat island of Nanjing, China." *Building and Environment* 43 (2008): 7-17.

IPCC. *IPCC Fourth Assessment Report: Climate Change 2007.* 2007. http://www.ipcc.ch/publications_and_data/ar4/wg1/en/spmsspm-direct-observations.html (accessed October 16, 2011).

Jensen, John R. *Remote Sensing of the Environment: An Earth Resource Perspective.* Upper Saddle River, NJ: Pearson Prentice Hall, 2007.

Jin, Menglin S. "Developing an index to measure urban heat island effect using satellite land skin temperature and land cover observations." *American Meteorological Society* 25, no. 18 (September 2012): 6193-6201.

Katsouyanni, K., A. Pantazopoulou, and G. Touloumi. "Evidence for the interaction between air pollution and high temperature in the causation of excess mortality." *Archives of Environmental Health* 48 (1993): 235-242.

Katzschner, Lutz., and Sofia Thorsson. "Microclimatic investigations as tool for urban design." Yokohama, Japan: Seventh International Conference on Urban Climate, 2009.

Ligda, M., and S. Bigler. *Use of radar in severe storm detection: hydrology and climatology.* Texas A&M University, 1956.

Lyndon State College Atmospheric Sciences. *Measuring Temperature.* September 9, 2005. http://apollo.lsc.vsc.edu/classes/met130/notes/chapter3/t_measure.html (accessed May 5, 2014).

McPherson, E.G. "Sacramento's parking lot shading ordinance: environmental and economic costs of compliance." *Landscape and Urban Planning* (UC Davis) 57 (2002): 105-123.

Oberndorfer, E., et al. "Green roofs as urban ecosystems: ecological structures, functions, and services." *Architectural Science Publications and Research* 57, no. 10 (2007): 823-833.

Oke, T.R. "The distinction between canopy and boudary layer heat islands." *Atmosphere* 14 (1976): 268-277.

Pease, Robert W., John E. Lewis, and Samuel I. Outcalt. "Urban terrain climatology and remote sensing." *Annals of the Association of American Geographers* 66, no. 4 (1976): 557-569.

Runnalls, K. E, and T. R. Oke. "Dynamics and controls of the near-surface heat island of Vancouver, British Columbia." *Physical Geography* 21 (2000): 283-304.

Saucier, W. J. "Texas-west gulf cyclones." *Monthly Weather Review* 77 (1949): 219-231.

Sullivan, J. & Collins, J. M. "The use of low-cost data logging temperature sensors in the evaluation of an urban heat island in Tampa, Florida." *Papers of the Applied Geography Conferences* 32 (2009): 252-261.

Taha, Haider. "Urban climates and heat islands: albedo, evapotranspiration, and anthropogenic heat." *Energy and Buildings* (Lawrence Berkely National Laboratory), no. 25 (1997): 99-103.

The Weather Channel. *Monthly Weather for Northridge, CA 91325.* 2012. http://www.weather.com/weather/wxclimatology/monthly/graph/91325 (accessed July 28, 2013).

Torok, Simon J, Christopher J.G Morris, Carol Skinner, and Neil Plummer. "Urban heat island features of southeast Australian towns." *Australian Meteorological Magazine* 50 (2001): 1-13.

Unger, Janos. "Connection between urban heat island and sky view factor approximated by a software tool on a 3D urban database." *International Journal of Environment and Pollution* 36 (2009): 59-80.

United Nations. "United Nations: Department of Economic and Social Affairs." *Urban and Rural Areas 2009.* New York: United Nations, June 2010.

United States Centers for Disease Control and Prevention. *Heat-Related Morbidity and Mortality.* November 29, 2010. http://www.cdc.gov/climatechange/effects/heat_related.htm (accessed October 16, 2011).

United States Environmental Protection Agency. *Water Sense/ Outdoor Water Use in the US.* December 19, 2013. http://www.epa.gov/WaterSense/pubs/outdoor.html (accessed December 31, 2013).

United States Environmental Protection Agency. *Reducing urban heat islands: compendium of strategies.* 2014. http://www.epa.gov/heatisland/resources/pdf/BasicsCompendium.pdf (accessed May 4, 2014).

Weng, Qihao. "Thermal infrared remote sensing for urban climate and environmental studies: Methods, applications, and trends." *International Society for Photogrammetry and Remote Sensing* 64 (2009): 335-344.

Woollum, C. A., and N. L. Canfield. *Washington Metropolitan Area Precipitation and Temperature Patterns Technical.* U.S Department of Commerce ESSA, 1968.

Zoulia, I., M. Santamouris, and A. Dimoudi. "Monitoring the effect of urban green areas on the heat island in Athens." *Environmental Monitoring & Assessment* 156 (2009): 275-292.